I&EC research
Industrial & Engineering Chemistry Research

pubs.acs.org/IECR

Article

Thermodynamic and Process Analyses of Extractive Distillation for Separating Refrigerant R-410A Using Imidazolium-Cyano-Based Ionic Liquids

Published as part of Industrial & Engineering Chemistry Research special issue "Phillip E. Savage Festschrift".

Julia E. Espinoza Mejia, Abdulrhman M. Arishi, Mark B. Shiflett, and Aaron M. Scurto*

Cite This: *Ind. Eng. Chem. Res.* 2025, 64, 672−691

Read Online

ACCESS | Metrics & More | Article Recommendations | Supporting Information

ABSTRACT: R-410A is a near-azeotropic refrigerant mixture of difluoromethane (HFC-32) and pentafluoroethane (HFC-125) that is scheduled to be phased out internationally due to a high Global Warming Potential (GWP). While conventional distillation cannot be used, extractive distillation using ionic liquids (ILs) has been proposed to separate and recycle HFC-32 (lower GWP) for future refrigerant blends and to repurpose HFC-125 (high GWP). Here, we present both a thermodynamic and process design analyses of various ILs using an equation of state method. From experimental binary vapor−liquid equilibrium data and equation of state modeling, 1-ethyl-3-methylimidazolium tricyanomethanide $[C_2C_1im][tcm]$ and 1-ethyl-3-methylimidazolium dicyanamide $[C_2C_1im][dca]$ were identified from 10 ILs as viable entrainers. Selectivity increases with temperature and decreases with pressure, while the solvent-to-feed (S/F) ratio did not have much effect. These effects were more pronounced for $[C_2C_1im][tcm]$ than for $[C_2C_1im][dca]$. A sensitivity analysis reveals that the optimum operational parameters were solvent-to-feed ratio (*S/F*), reflux ratio (*RR*), and total number of stages (*Nt*) with values of 5, 3, and 20, respectively, for the case of $[C_2C_1im][tcm]$ and 6, 3, and 20 for $[C_2C_1im][dca]$. High-purity products HFC-32 and HFC-125 (>99.5 wt %) were obtained with IL $[C_2C_1im][tcm]$, providing the lowest energy consumption, compared to $[C_2C_1im][dca]$ and other ILs.

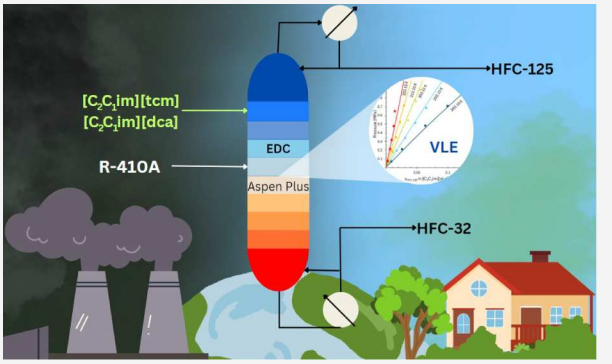

1. INTRODUCTION

Historically, refrigerants have contributed to the development of important industrial sectors such as residential and commercial cooling and heating, refrigeration and preservation of food and beverages, storage of pharmaceuticals, manufacturing of petrochemicals, and more recently, cooling data centers.[1−4] Even though refrigeration is considered one of the most important accomplishments of the 20th century, many of the refrigerants used today are hydrofluorocarbons (HFCs), which are potent greenhouse gases.[5−8] The global warming potential (GWP) of many HFCs is thousands of times greater than carbon dioxide as a consequence of their extended infrared radiation absorption spectra and long atmospheric lifetimes.[9−12] The American Innovation and Manufacturing (AIM) Act and the Kigali amendment to the Montreal Protocol require that many high-GWP HFC refrigerants be phased down over the next two decades and replaced with low-GWP options such as hydrofluoroolefin (HFO) refrigerants and HFO/HFC blends.[13−15] Most commercial refrigerants sold today are azeotropic or near-azeotropic mixtures that are difficult to separate using incumbent technology based on fractional distillation. In addition, the Environmental Protection Agency (EPA) has proposed that by 2028, certain new equipment must be charged with a portion of recycled refrigerant.[16] This has created concern in the Heating, Ventilation, Air-Conditioning, and Refrigeration (HVACR) industry, given that less than 3% of refrigerants entering the market today are recycled.[17,18] New technologies are needed to separate azeotropic refrigerant mixtures into pure components that meet industry specifications (e.g., AHRI 700 standard).[19−22] Effective and industrially scalable separation techniques for increasing the amount of recycled refrigerants are urgently needed[23,24]

Many innovative and sustainable solutions have been proposed for the separation of azeotropic HFC blends. Some examples include selective adsorption using porous materials such as zeolites, activated carbons, and metal−organic structures;[25−29] membrane separation using polyimides and

Received: August 30, 2024
Revised: November 27, 2024
Accepted: December 5, 2024
Published: December 24, 2024

fluoropolymers,[30−34] and extractive distillation using ionic liquids (ILs) as entrainers.[35−41] Other, more traditional techniques, such as cryogenic distillation, are not effective for separating azeotropic mixtures and are highly energy-intensive and expensive to operate.[42−45] In contrast, ILs show promise for separating azeotropic refrigerant mixtures using extractive distillation technology.[46−48] Since the early 2000, ILs have been investigated for use with refrigerants in this application owing to their exceptional properties, such as negligible vapor pressure, a wide liquid temperature range, high thermal and chemical stability, and enhanced solvation properties, among others. A myriad of cation and anion configurations exist for designing ILs for specific absorption processes.[49−52] Designing extractive distillation systems for ILs and HFC refrigerants with similar boiling points requires accurate thermodynamic and transport properties.[53−55]

Many studies on refrigerant/IL binary systems have focused on measuring and modeling thermodynamic properties, such as global phase behavior and phase equilibrium (i.e., vapor−liquid equilibria (VLE), vapor−liquid−liquid equilibria (VLLE), and liquid−liquid-equilibria (LLE)).[56−65] Shiflett and coworkers were the first to measure and model the gas solubility of HFC refrigerants in ILs.[66−68] Several thermodynamic methods incorporating activity coefficient models, e.g., the nonrandom two-liquid (NRTL) activity coefficient model, and/or cubic Equation of State (EoS) models, such as the Redlich−Kwong and Peng−Robinson models, have been successfully applied.[53,55,66,67,69−71] More recently, new approaches are being utilized that include quantum chemistry,[72,73] molecular dynamics simulations,[74,75] artificial neural networks,[76,77] and the Statistical Associating Fluid Theory (SAFT) equations of state.[78] A recent review on the separation of fluorocarbons using ILs provides an up-to-date summary of the experimental and computationally studies of various ILs and fluorinated hydrocarbons.[18] One observation was that ILs containing fluorinated anions have greater solubility for fluorinated hydrocarbons,[79] and cyano-based ILs tend to increase fluorinated hydrocarbons solubility even more.[80] Further understanding of the phase behavior of refrigerants in ILs, particularly the solubility of ternary systems (i.e., two refrigerants in the same IL), is needed to properly model and optimize ILs for extractive distillation processes.

Shiflett and Yokozeki initially proposed the use of 1-butyl-3-methylimidazolium hexafluorophosphate ($[C_4C_1im][PF_6]$) for the separation of the refrigerant mixture R-410A also known commercially as Genetron AZ-20, EcoFluor R410, Forane 410A, Puron R410A, and Suva 410A.[69] R-410A is a near-azeotropic mixture of 50 wt % difluoromethane (HFC-32, R-32, CH_2F_2) and 50 wt % pentafluoroethane (HFC-125, *R*-125, CHF_2CF_3). HFC-32 has a relatively low-GWP (GWP_{100} = 675) compared to HFC-125 with a high-GWP (GWP_{100} = 3500). If HFC-32 can be separated from R-410A, it can be used to produce new low-GWP blends with HFOs such as R-454A, R-454B, and R-454C. R-454B is a proposed replacement for R-410A and is composed of 69.9 wt % HFC-32 and 31.1 wt % 2,3,3,3-tetrafluoropropene (HFO-1234yf, $CH_2{=}CFCF_3$) with a 78% lower GWP (GWP_{100} = 466) compared with R-410A (GWP_{100} = 2088).[81] A few studies have evaluated the separation of R-410A using ILs as entrainers in extractive distillation;[39,41,42,82,83] however, the challenge of producing high-purity HFC-32 and HFC-125 (i.e., >99.5 wt %) remains. 99.5 wt % is the minimum industrial purity allowed for reuse/resale.[84] New ILs are being developed with the goal of producing the highest purity products with the lowest energy consumption (i.e., lowest operating costs). For example, Finberg and Shiflett assessed 1-butyl-3-methylimidazolium hexafluorophosphate $[C_4C_1im][PF_6]$ and 1-ethyl-3-methylimidazolium bis(trifluoromethylsulfonyl)imide $[C_2C_1im][Tf_2N]$ and simulated purities of 99.6 and 99.5 wt %, respectively, for both HFC-125 and HFC-32.[39] Likewise, Monjur et al. also evaluated $[C_4C_1im][PF_6]$ as an entrainer for separating R-410A and obtained a purity of 99.5 and 99.8 wt % for HFC-125 and HFC-32, respectively.[42] Asensio-Delgado et al. evaluated the separation of R-410A using $[C_2C_1im][Tf_2N]$ as a solvent and reported 99.5 and 84.0 wt % purity of HFC-125 and HFC-32, respectively.[83] Ye et al. was able to produce 99.5 wt % purities for both HFC-125 and HFC-32 using $[C_2C_1im][Tf_2N]$.[82] Cyano-based ILs, such as 1-ethyl-3-methylimidazolium thiocyanate ($[C_2C_1im][SCN]$), have been investigated by Viar et al., achieving a purity of 99.5 wt % for both HFC-125 and HFC-32.[41] Similar results were found by Ye et al. when testing IL $[C_2C_1im][SCN]$.[82] Even though targeted purities were achieved with different ILs in most cases, the number of column stages and working pressures were significantly lower in the case of cyano-based ILs. In addition, higher ideal selectivity has been reported for cyano-based ILs; therefore, further evaluation is needed for cyano-based ILs as entrainers in the extractive distillation process design for the separation of R-410A.

In this work, cyano-based ILs are simulated as entrainers in extractive distillation processes for R-410A separations. Specifically, 1-ethyl-3-methylimidazolium dicyanamide $[C_2C_1im][dca]$ and 1-ethyl-3-methylimidazolium tricyanomethanide $[C_2C_1im][tcm]$ were evaluated for the separation of R-410A as entrainers using extractive distillation. A detailed comparison of these results with previous works has also been included to compare the performance and overall energy consumption. Furthermore, the effect of temperature, pressure, and solvent-to-feed ratio on selectivity was analyzed for ternary systems.

2. COMPUTATIONAL DETAILS

In general, the process simulation model was built by performing the following necessary steps: (1) specify the chemical components (i.e., HFC-32, HFC-125, ILs $[C_2C_1im][tcm]$, and $[C_2C_1im][dca]$), specify the thermodynamic model (i.e., PR EoS combined with the Boston-Mathias alpha functionality and mixing rule); (2) perform a binary VLE regression (i.e., HFC-32/$[C_2C_1im][tcm]$, HFC-125/$[C_2C_1im][tcm]$, and HFC-32/$[C_2C_1im][dca]$, HFC-125/$[C_2C_1im][dca]$); (3) define the process flowsheet (i.e., extractive distillation system); (4) include flow rates and thermodynamic conditions for all streams and unit operation blocks (i.e., column, reboiler, condenser, flash tank, heat exchangers, and others); and (5) perform a sensitivity analysis for optimizing operational parameters (feed stage, solvent-to-feed-ratio, reflux-ratio, total number of stages). A detailed description of the VLE regression used in this work has been discussed in detail in previous publications.[35−39] The Aspen Plus V14 process simulator was used to develop an extractive distillation model using a rigorous Aspen Radfrac column.

2.1. Component Specification. The ILs $[C_2C_1im][tcm]$ and $[C_2C_1im][dca]$ were created as user-defined components. To complete the specification for both ILs, the pseudo physical and critical properties, as well as ideal gas heat capacities, were calculated using the group contribution method.[85,86] The critical properties of ILs cannot be measured because they decompose before reaching such high temperatures, so the group

https://doi.org/10.1021/acs.iecr.4c03268
Ind. Eng. Chem. Res. 2025, 64, 672−691

Table 1. Physical and Critical Pseudo Properties for ILs

CAS No.	IL	MW (g mol^{-1})	T_b (K)	T_c (K)	P_c (MPa)	ω
370865-89-7	[C_1C_2im][dca]	177.20	737.20	999.00	2.91	0.77
666823-18-3	[C_1C_2im][tcm]	201.23	858.69	1141.22	2.46	0.81

Table 2. Binary Interaction Parameters and Average Absolute Deviations

		Binary Interaction Parameters				Average Absolute Relative Deviation (% AARD)		
Component j	Component i	$k_{ij}^{(1)}$	$k_{ij}^{(2)} \times 10^3$ (K^{-1})	$l_{ij}^{(1)}$	$l_{ij}^{(2)} \times 10^3$ (K^{-1})	T	P	x_i
[C_2C_1im][tcm]	HFC-125	0.118	−0.281	0.941	−3.389	0.068	0.062	6.123
	HFC-32	0.035	−0.077	0.037	−0.008	0.009	0.012	1.221
[C_2C_1im][dca]	HFC-125	−0.124	0.571	0.648	−2.45	1.117	0.067	6.804
	HFC-32	−0.046	0.25	−0.105	0.409	0.166	0.018	1.932
HFC-32	HFC-125	0.0155	−0.05	0.0981	−0.280	2.25	0.219	0.001

contribution method was used to calculate the pseudo properties.[87,88] The physical and critical properties of the ILs are shown in Table 1.

2.2. VLE Regression. The PR EoS, combined with the van der Waals two-parameters mixing rule and the Boston-Mathias alpha functionality,[89,90] as implemented in Aspen Plus, was selected to model the VLE phase equilibrium of HFC-32 and HFC-125 in ILs [C_2C_1im][tcm] and [C_2C_1im][dca] (binary mixtures). Previous studies have shown the accuracy of the Peng−Robinson Boston-Mathias van der Waals two-parameters (PR-BM-vdW-2) property method with respect to the classical thermodynamic model NRTL for regressing VLE experimental data (e.g., HFC-32 and HFC-125 in ILs).[64,91] In this work the temperature-dependent binary interaction parameters (BIP's) k_{ij} and l_{ij} are assumed to be symmetric ($k_{ij} = k_{ji}$ and $l_{ij} = l_{ji}$). The BIP's and average absolute relative deviations (AARD) obtained from the VLE regression are shown in Table 2. Thermodynamic equations and the complete methodology for BIP's have been described in our previous work.[35−39]

The regression algorithm utilizes the Maximum Likelihood (ML) objective function, which is a generalization of the least-squares method. In the least-squares method, the independent variables are assumed to be error-free, and errors in the dependent parameters are minimized by adjusting one or more model parameters. In contrast, the ML method considers errors in all variables; therefore, the objective function is minimized by manipulating the regressed parameters (i.e., binary interaction parameters, k_{ij} and l_{ij}) and the estimated values corresponding to each measurement, subject to the constraints of phase equilibrium.[92] The ML objective function is shown in eq 1.[93,94]

$$Q = \sum_{d=1}^{D}\sum_{i=1}^{N}\left[\left(\frac{T_{e,i} - T_{r,i}}{\sigma_{T,i}}\right)^2 + \left(\frac{P_{e,i} - P_{r,i}}{\sigma_{P,i}}\right)^2 + \sum_{j=1}^{NC}\left(\frac{x_{e,i,j} - x_{r,i,j}}{\sigma_{x,i,j}}\right)^2\right] \quad (1)$$

where Q is the objective function to be minimized by data regression, D is the total number of data groups used, d is the number of data groups in the regression case, N is the total number of points in a data group, NC is the number of components present in a data group, T, P, and z, are the temperature, pressure, and total mole fraction, e is the experimental data, r is the regressed data, i indicates the data point "i", j indicates the fraction data for component "j", and σ stands for standard deviation of the indicated data.

For the binary VLE, only two degrees of freedom are needed for defining the system. The PR-BM-vdW-2 model chosen will estimate T_r based on experimental P_e and z_e, similarly P_r is estimated based on T_e and x_e, and x_r is estimated based on experimental P_e and T_e. Contrary to the classic least-squares method, where the error is minimized for each set of experimental data points under the assumption that they are not affected by error, in the ML method, the regression is performed to make the experimental data the most likely when considered as a whole. Regressions based on the ML objective function have been shown to present advantages over the classical least-squares method in the reduction of VLE data.[92] The ML method constraints are shown in Table 3.[95]

Table 3. ML Objective Function Constrains

Status	Constraint
Actual Constraints	$\Phi_i^v y_i P - \Phi_i^l x_i P = 0$
Implicit Constraints	$\Phi_i^v = \Phi_i^v(T, P, y)$
	$\Phi_i^l = \Phi_i^l(T, P, x)$
	$f_i^v = f_i^v(T, P, y)$
	$f_i^l = f_i^l(T, P, x)$
	$\sum z_i = 1$
	$\sum x_i = 1$
	$\sum y_i = 1$

The PTx diagrams for HFC-32 and HFC-125 in [C_2C_1im]-[tcm] and [C_2C_1im][dca], respectively, are shown in Figure 1. Experimental data are taken from Asensio-Delgado et al.[59] Predicted values from the PR-BM-vdW-2 model are found to be in good agreement with the experimental values. Large standard deviations of estimated parameters do not necessarily indicate a poor fit; however, a residual value much larger than the others might indicate a "bad" data point. The residual root-mean-square error ($RRMSE$) is defined in eq 2.

$$RRMSE = \sqrt{\frac{Q}{K - n}} \quad (2)$$

where Q is the objective function to be minimized by data regression, K is the number of data points, and n is the total number of model parameters. Normally the RRMSE value should be less than 10 for VLE data and less than 100 for LLE data.[93] Using experimental VLE data from literature,[41,57,59,66,96] eight other ILs ([C_4C_1im][tcm], [C_6C_1im][tcm], [C_8C_1im]-

https://doi.org/10.1021/acs.iecr.4c03268
Ind. Eng. Chem. Res. 2025, 64, 672−691

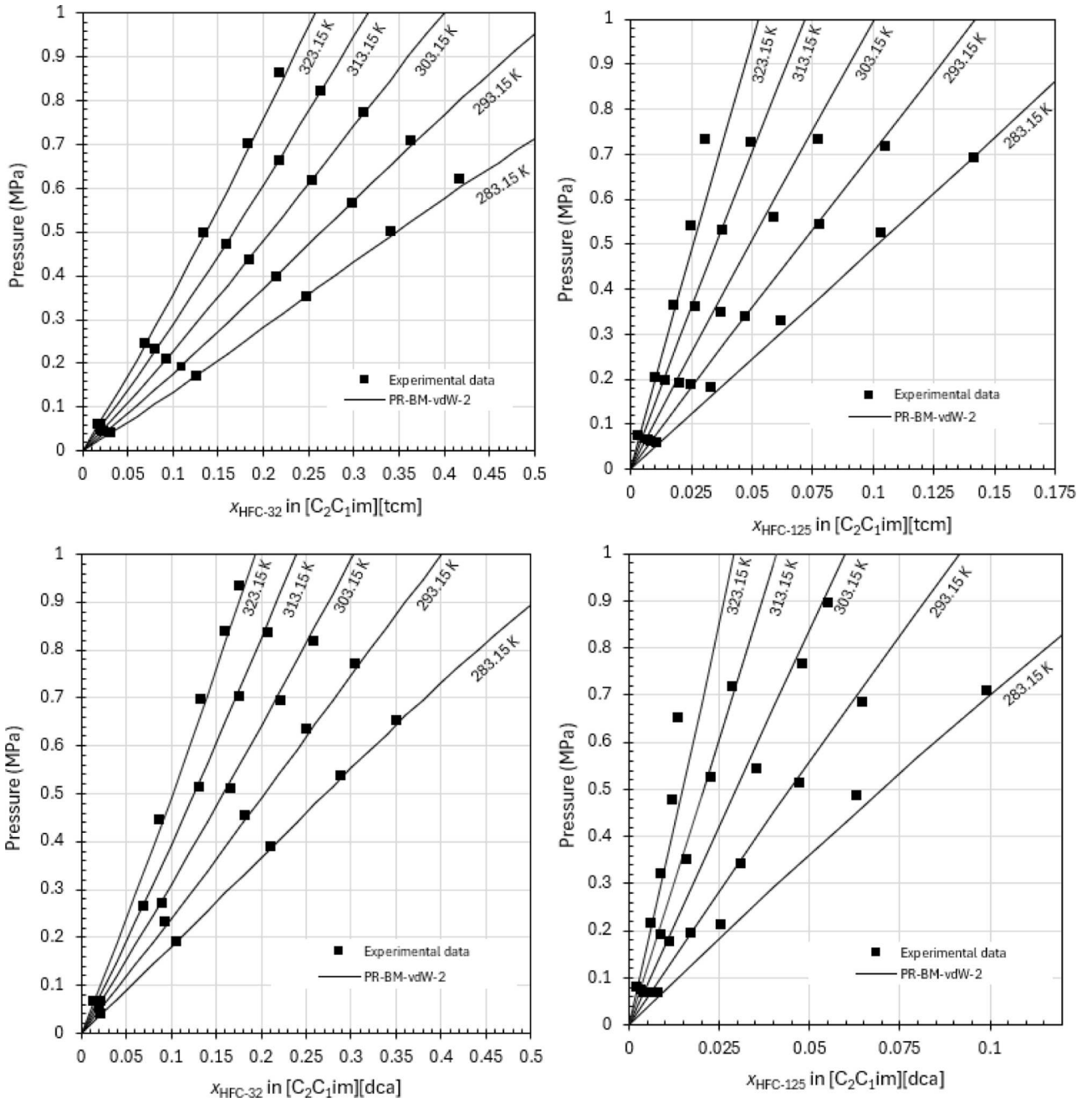

Figure 1. *PTx* diagrams for HFC-32 and HFC-125 in [C_2C_1im][tcm] and [C_2C_1im][dca]. Experimental data (black squares) and the PR-BM-vdW-2 EoS model (solid lines).

[tcm], [C_4C_1im][dca], [C_2C_1im][SCN], [C_2C_1im][Tf_2N], [C_2C_1im][BF_4], [C_4C_1im][PF_6]) were regressed using the PR-BM-vdW-2 model[89,90] and the *PTx* diagrams are shown in Figures 1S−8S.

2.3. ASPEN RADFRAC Modeling. ASPEN RADFRAC is a rigorous model commonly used for many types of multistage vapor−liquid (VL) and VLL fractioning operation units.[97,98] In this case, VL was chosen as a valid phase. The extractive distillation column was simulated by using the Aspen Plus V14 RADFRAC model that includes a condenser and a reboiler. The RADFRAC model estimates the temperature profile in the column based on the bubble and dew point of the feed components. Likewise, the RADFRAC columns can be simulated using either the design or rating modes. The mass transfer calculations can be addressed from an equilibrium or rate-based model. This work developed a design-equilibrium model with strongly nonideal liquid convergence. In equilibrium modeling, the pumping requirements will be minimum due to the lack of viscosity inputs. The reboiler was chosen to operate as a kettle with a total condenser, and vapor−liquid equilibrium was set as the valid phases. Additional information about the constraints and heuristics established for this work is included in Section 3. A general process configuration is shown in Figure 2.

3. SIMULATION OPTIMIZATION

3.1. Constraints and Heuristics. To limit the number of variables used for optimizing the process, constraints and heuristics need to be defined. In this work, the feed flow rate of R-410A was set at 10 kg/h (rate recommended for a 7.62 cm (3

https://doi.org/10.1021/acs.iecr.4c03268
Ind. Eng. Chem. Res. 2025, 64, 672−691

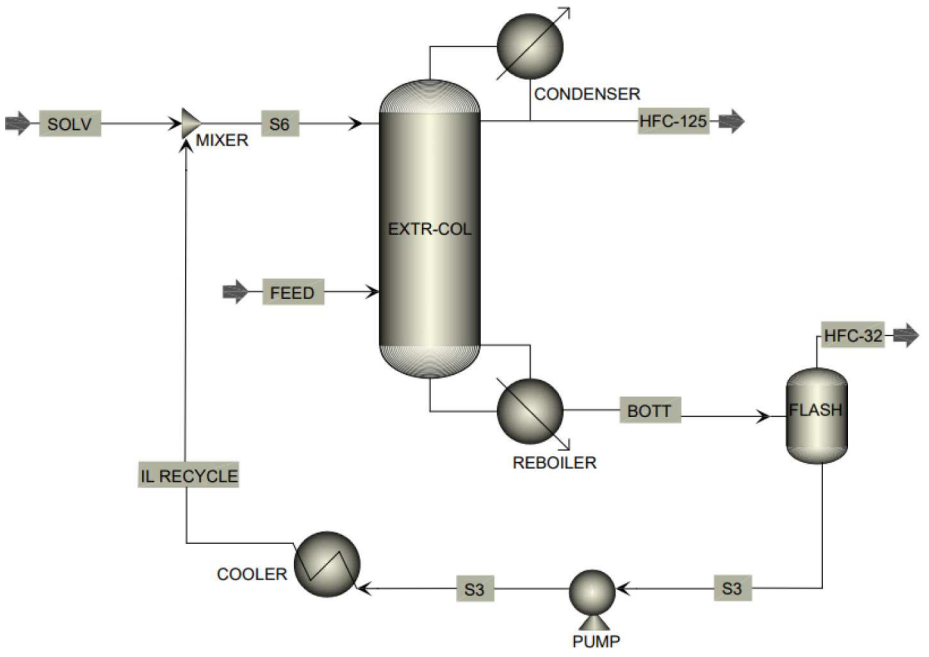

Figure 2. Extractive Distillation Process Configuration Diagram.

in.) diameter pilot-scaled column) and 293.15 K (ambient temperature). The maximum reboiler temperature was limited to be lower than 443.15 K, which corresponds to the IL thermal degradation onset temperature for cyano-containing ILs.[99,100] Because of the negligible vapor pressure of ILs, in the column, stage 2 was considered as the IL inlet to maximize the contact area between the solvent and the refrigerants. Likewise, stage 1 was designated as the total condenser. The chosen ILs preferentially absorb HFC-32, thus HFC-125 becomes concentrated in the distillate stream, while HFC-32 flows to the bottom of the column with the IL. The distillate stream flow rate was kept constant at 5 kg/h. A flash tank was used to remove the enriched HFC-32 from the IL and was kept at a constant temperature of 373.15 K and pressure of 0.1 MPa to enhance the HFC-32 separation from the IL. The goal is to recover HFC-32 and HFC-125 with a minimum purity of 99.5 wt %, which meets the AHRI 700 specification for recycled refrigerants.[84]

3.2. Sensitivity Analysis. A detailed sensitivity analysis for optimizing the extractive distillation process was described in our previous work, and so we have provided only a few of the more important details here.[35−39] An algorithm is shown in Figure 3, where the solvent-to-feed ratio (S/F), total number of stages (N_t), the feed stage (N_f), reflux ratio (RR), column pressure (P), and HFC-125 composition ($x_{\text{HFC-125}}$) are the parameters used for the process optimization.

The sensitivity analysis in this work begins by defining initial values taken from our previous work (e.g., $S/F = 6$, $N_t = 20$, and $RR = 3$).[35−39] With these parameters fixed, the refrigerant composition (i.e., $x_{\text{HFC-125}}$ or $x_{\text{HFC-32}}$) is varied with respect to the feed stage at different column pressures. The refrigerant targeted purity (99.5 wt %) will determine the optimal N_f and the minimum P. By knowing the optimal feed stage, this parameter can be fixed, and the refrigerant composition can be varied with respect to the S/F ratio at different p values by holding constant the RR. The refrigerant targeted purity (99.5 wt %) will determine the S/F ratio and the minimum P. Holding the S/F ratio fixed, the $x_{\text{HFC-125}}$ can be varied with respect to the RR as a function of P. The $x_{\text{HFC-125}}$ purity (99.5 wt %) will

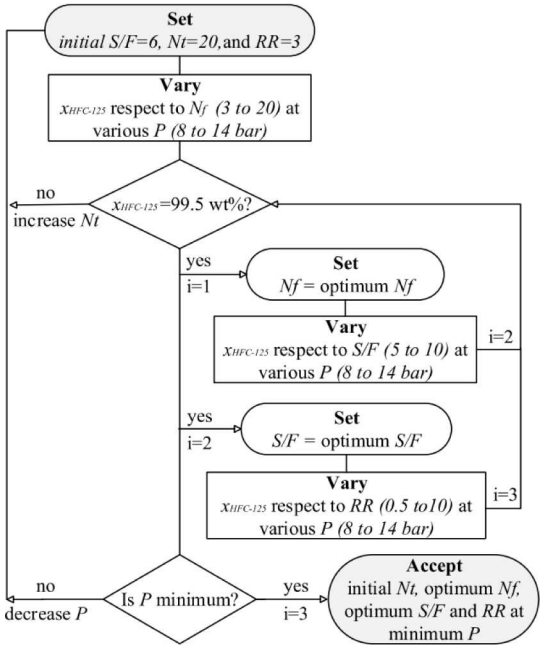

Figure 3. Flowchart for optimizing the process simulation. Initial parameters are defined from typical process heuristics.

determine the RR ratio and the minimum P. If these conditions are not fulfilled, the loop restarts by setting up another P or increasing Nt.

4. RESULTS AND DISCUSSION

4.1. Ionic Liquid Selection. *4.1.1. Solubility.* Solubility and selectivity are two terms commonly used in selecting materials for separation performance. Ideally, the optimal IL would have high solubility for one of the refrigerant components and low solubility for the other components to ensure maximum separation. The total solubility is generally called the absorption capacity. However, the solubility of HFCs in some ILs has

https://doi.org/10.1021/acs.iecr.4c03268
Ind. Eng. Chem. Res. 2025, 64, 672−691

shown a highly nonlinear relationship, which varies with the IL, temperature, and pressure. VLE behavior for HFC/IL systems is generally nonlinear outside the initial "Henry's Law" regime. Therefore, the difference in solubility of one refrigerant versus another must be analyzed under specific operational conditions. A straightforward way to compare the selectivity of different ILs is by measuring and modeling the solubility differences of the refrigerant components. The solubility difference of HFC-32 and HFC-125 in ten ILs commonly used for R-410A separation is shown in Table 4 and Figure 4.

Table 4. HFC Solubility and HFC Solubility Difference in ILs at 0.5 MPa and 303.15 K

Ionic liquid	HFC-32 solubility	HFC-125 solubility	Solubility difference (HFC-32- HFC125)
$[C_4C_1im][PF_6]$	0.305	0.119	0.186
$[C_2C_1im][Tf_2N]$	0.343	0.231	0.112
$[C_8C_1im][tcm]$	0.248	0.098	0.150
$[C_6C_1im][tcm]$	0.236	0.080	0.155
$[C_4C_1im][tcm]$	0.218	0.062	0.156
$[C_2C_1im][tcm]$	0.211	0.050	0.161
$[C_2C_1im][BF_4]$	0.195	0.074	0.121
$[C_4C_1im][dca]$	0.185	0.052	0.133
$[C_2C_1im][dca]$	0.151	0.050	0.101
$[C_2C_1im][SCN]$	0.124	0.019	0.105

The experimental VLE data were taken from literature,[41,57,59,66,96] and regressed using the PR-BM-vdW-2 model[89,90] at 303.15 K and 0.5 MPa. These conditions are relatively close to the actual operating conditions of a pilot-scale extractive distillation column that we have at the University of Kansas (KU). It is important to mention that evaluating the performance at atmospheric pressure and temperature (i.e., 0.1 MPa and 298.15 K) can lead to different conclusions. Maximizing the solubility difference between HFC-32 and HFC-125 is one method for choosing an IL entrainer for extractive distillation. For example, the solubility of one component is maximized with as large a solubility difference as possible. In this case, $[C_4C_1im][PF_6]$ shows the largest solubility difference (0.186 mole fraction). Tricyano-based ILs $[C_2C_1im][tcm]$, 1-butyl-3-methylimidazolium tricyanomethane $[C_4C_1im][tcm]$, 1-hexyl-3-methylimidazolium tricyanomethanide $[C_6C_1im][tcm]$, and 1-octyl-3-methylimidazolium tricyanomethanide $[C_8C_1im][tcm]$ have similar and the second largest solubility difference. The trend is followed by 1-butyl-3-methylimidazolium dicyanamide $[C_4C_1im][dca]$, 1-ethyl-3-methylimidazolium tetrafluoroborate $[C_2C_1im][BF_4]$, $[C_2C_1im][Tf_2N]$, 1-ethyl-3-methylimidazolium thiocyanate $[C_2C_1im][SCN]$, and $[C_2C_1im][dca]$ (0.101 mole fraction), as shown in Figure 4.

In general, HFC-32 solubility in the 10 ILs evaluated at 0.5 MPa and 303.15 K follows the order: $[C_2C_1im][Tf_2N]$ > $[C_4C_1im][PF_6]$ > $[C_8C_1im][tcm]$ > $[C_6C_1im][tcm]$ > $[C_4C_1im][tcm]$ > $[C_2C_1im][tcm]$ > $[C_2C_1im][BF_4]$ ≈ $[C_4C_1im][dca]$ > $[C_2C_1im][dca]$ > $[C_2C_1im][SCN]$. Similarly, for HFC-125 solubility at 0.5 MPa and 303.15 K, the order is: $[C_2C_1im][Tf_2N]$ > $[C_4C_1im][PF_6]$ > $[C_8C_1im][tcm]$ > $[C_6C_1im][tcm]$ ≈ $[C_2C_1im][BF_4]$ > $[C_4C_1im][tcm]$ > $[C_4C_1im][dca]$ ≈ $[C_2C_1im][tcm]$ > $[C_2C_1im][SCN]$. It is found that HFC-32 is more soluble in any given IL compared to HFC-125. In extractive distillation, HFC-125 would be considered as the light key component and HFC-32 as the heavy key component. As a rule, high solubility would help the "capacity", i.e., the ability of the IL entrainer to absorb gas.

4.1.2. Ideal Selectivity. While high capacity is sought, it is also preferrable that the solubility of HFC-32 in the IL is much higher than the solubility of HFC-125, i.e., high selectivity (eq 3). While an actual extractive distillation system to separate a gas mixture would be a ternary system ($HFC_1/HFC_2/IL$), the ideal selectivity based only on a binary system (HFC/IL) is also useful for IL selection.[59,66,71,101] The ideal selectivity is expressed as follows:

$$S_{i,j}^{\text{Ideal}}(T, P) = \frac{K_i(T, P)}{K_j(T, P)} = \left(\frac{y_i/x_i}{y_j/x_j}\right) = \left(\frac{x_j}{x_i}\right) \tag{3}$$

where subscript "i" and "j" refer to the component i (i.e., HFC-125) and the component j (i.e., HFC-32), K_i and K_j represent the distribution coefficients, and x and y are the liquid and gas mole fractions of the dissolved refrigerant in the IL, respectively. As the IL is nonvolatile, the vapor phase composition of the HFCs is considered equal to 1 ($y_i = 1$) for binary-VLE cases. An ideal selectivity that is far from unity is desired, as this difference, which is the extraction of one gas over the other, would yield a more efficient separation.

The ideal selectivity as a function of HFC-32 solubility in 10 ILs was calculated based on experimental VLE data found in the literature,[41,57,59,66,96] and regressed using the PR-BM-vdW-2 model at 0.5 MPa and 303.15 K. The trade-off between HFC-32 solubility (capacity) and ideal selectivity are represented as a single point, and the HFC-32 solubility−ideal selectivity maximization is shown in a Pareto front (dashed line) in Figure 5. For the HFC-125/HFC-32 blend, the ideal selectivity in different ILs is greater than 1 in all cases and the order is: $[C_2C_1im][SCN]$ > $[C_2C_1im][tcm]$ > $[C_4C_1im][tcm]$ ≈ $[C_4C_1im][dca]$ > $[C_2C_1im][dca]$ ≈ $[C_6C_1im][tcm]$ > $[C_2C_1im][BF_4]$ ≈ $[C_8C_1im][tcm]$ ≈ $[C_4C_1im][PF_6]$ > $[C_2C_1im][Tf_2N]$. The best ideal selectivity was found for the HFC-125/HFC-32 blend in $[C_2C_1im][SCN]$ at 0.5 MPa and 303.15 K; however, it also shows the lowest HFC-32 solubility, which means low recovery. Additionally, Viar et al. have found that the HFC-125/HFC-32 blend in $[C_2C_1im][SCN]$ shows the highest selectivity among other ILs at 1.4 MPa and 318.15 K.[41] Ye et al. have also found $[C_2C_1im][SCN]$ to exhibit the highest selectivity at infinite dilution at 298.15 K in comparison with other 22 ILs.[82] Although many authors have highlighted the high selectivity of $[C_2C_1im][SCN]$, its use may be limited by its chemical stability. Li and Pistorius concluded that $[SCN]^-$-based ILs can produce sulfide corrosion products with stainless steel.[102−105] Metal leaching from stainless steel when using $[SCN]^-$ ILs was also observed in our lab.

Due to the limited solubility data of the HFC-125/HFC-32 blend with other ILs at moderate-high pressures (i.e., ≥ 0.5 MPa), selectivities cannot be compared with other researchers' findings (as most of these studies were conducted at infinite dilution under ambient temperatures and pressures). $[C_2C_1im][tcm]$ has the highest ideal selectivity (4.244) among the ILs with HFC-32 solubility higher than 0.15 ($[C_2C_1im][tcm]$, $[C_2C_1im][dca]$, $[C_4C_1im][tcm]$, $[C_4C_1im][dca]$). Therefore, the hypothesis is that this IL will offer the best performance as an entrainer.

4.1.3. Ternary System Predictions. Unfortunately, there is only one publication regarding experimental ternary VLE data for the HFC-32, HFC-125 in $[C_4C_1im][BF_4]$ or $[C_4C_1im][PF_6]$, and only at a very low S/F ratio ($S/F \ll 1$) which would

https://doi.org/10.1021/acs.iecr.4c03268
Ind. Eng. Chem. Res. 2025, 64, 672−691

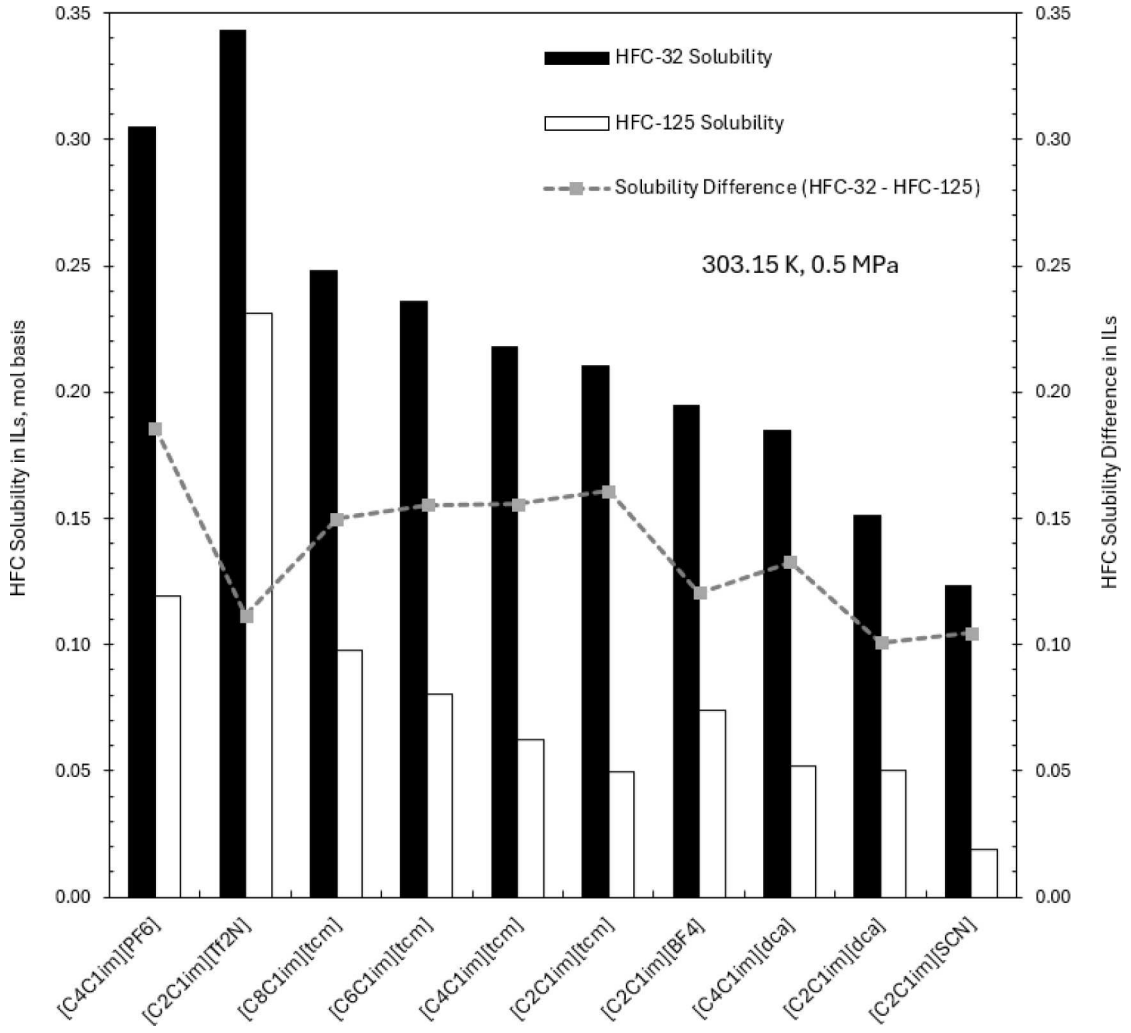

Figure 4. HFC solubility and HFC solubility difference in ILs at 0.5 MPa and 303.15 K. The black bars correspond to HFC-32 solubility (left axes), the white bars correspond to HFC-125 solubility (left axes), and the dashed line corresponds to the solubility difference between HFC-32 and HFC-125 in ILs (right axes).

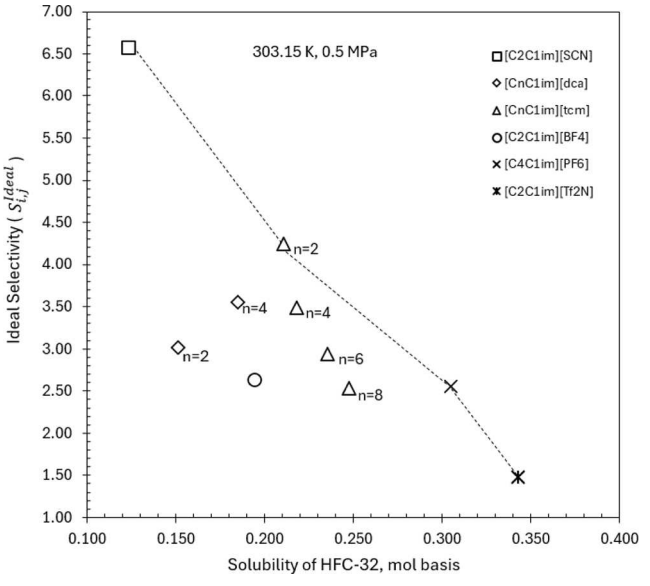

Figure 5. Ideal selectivity vs solubility of HFC-32 in a Pareto front at 0.5 MPa and 303.15 K.

be quite different than in an extractive distillation column.[106] However, an equation of state model can be used to predict these ternary mixtures based on binary VLE modeling. As HFC-125 and HFC-32 form a binary azeotrope, the main task of the entrainer IL is to shift the separation factor or selectivity as far from unity as possible, e.g., $S_{i,j} \gg 1$. A higher entrainer concentration (solvent-to-feed ratio) usually improves selectivity (see below). However, higher flow rates lead to higher IL inventories, higher pumping rates (electricity), and more cooling cost.

In a real situation, the ternary system HFC-125 (1)/HFC-32 (2)/IL (3) at 0.5 MPa and 303.15K will split into two phases in equilibrium (VLE). From the Gibbs phase rule, three degrees of freedom are required to define the three-components/two-phases equilibrium, and after temperature and pressure are chosen, the loading (z_i) or the components' overall compositions in the mixture are needed to determine tie-lines. The loading z_i is based upon the ratio of IL to gas feed (*R*-410A). Then, selectivity of HFC-125 (1)/HFC-32 (2), $S_{1,2}$ can be calculated according to eq 4.

$$S_{1,2}(T, P, z) = \frac{K_1(T, P, z)}{K_2(T, P, z)} = \left(\frac{(y_1/x_1)}{(y_2/x_2)}\right) \quad (4)$$

https://doi.org/10.1021/acs.iecr.4c03268
Ind. Eng. Chem. Res. 2025, 64, 672−691

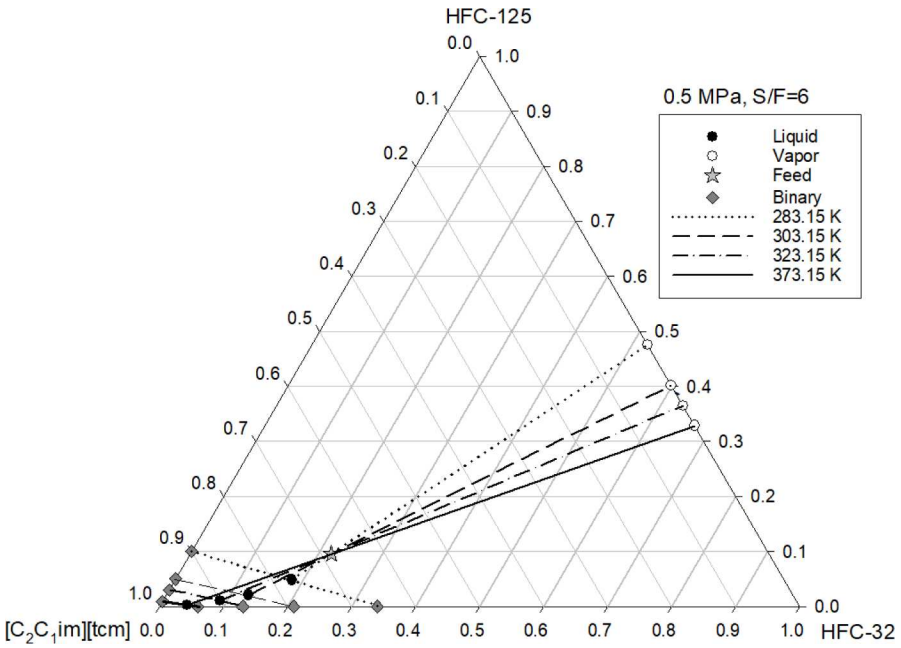

Figure 6. Temperature effect on solubility (mol basis) for HFC-125/HFC-32/[C_2C_1im][tcm] at 283.15, 303.15, 323.15, and 373.15 K at 0.5 MPa and S/F = 6 (mass basis; star). Isothermal lines between the binary VLE data are drawn to aid visualization.

Table 5. Selectivities, $S_{1,2}$, for Binary and Ternary Bases at Constant Pressure and S/F Ratio from the Model[a]

	Selectivity (mol basis) at 0.5 MPa and S/F = 6 (mass basis)					
	283.15 K		303.15 K		323.15 K	
IL	Binary	Ternary	Binary	Ternary	Binary	Ternary
[C_4C_1im][PF_6]	1.905	(*)	2.559	2.409	2.946	2.946
[C_2C_1im][Tf_2N]	1.343	(*)	1.483	1.500	1.560	1.591
[C_8C_1im][tcm]	1.996	2.298	2.529	2.914	3.093	3.427
[C_6C_1im][tcm]	2.406	2.248	2.939	2.857	3.472	3.458
[C_4C_1im][tcm]	2.650	2.726	3.494	3.461	4.398	4.281
[C_2C_1im][tcm]	3.451	3.294	4.244	3.930	5.311	4.800
[C_2C_1im][BF_4]	3.347	2.798	2.630	2.254	2.294	2.037
[C_4C_1im][dca]	2.421	2.357	3.554	3.458	4.513	4.473
[C_2C_1im][dca]	3.039	2.874	3.011	2.959	3.019	2.979
[C_2C_1im][SCN]	4.404	3.149	6.569	5.173	8.290	7.183

[a](*) At these conditions (0.5 MPa, 283.15 K, and S/F = 6), the loading is predicted to be subsaturated and forms a single liquid phase.

were K_1 and K_2 are the ternary distribution coefficients of HFC-125 and HFC-32, respectively. K_1 and K_2 are functions of the temperature, pressure, and the "loading" composition, z. Unlike the binary-based ideal selectivity, the vapor-phase compositions are not equal to one due to the mixed gas. In an extractive distillation system or in a one-stage flash system, the solvent-to-feed (S/F) ratio is usually specified. An S/F ratio of IL to R-410A of 6 on a mass basis corresponds to an overall mole fraction feed composition of 0.220 (mass fraction of 0.071) of HFC-32, 0.096 (0.071) of HFC-125, and 0.684 (0.857) of IL [C_2C_1im][tcm] (indicated as a star in Figure 6).

It is important to highlight that selecting an IL to perform a separation becomes difficult using only HFC-32 solubility (capacity) and ideal selectivity (separation factor), as these values are remarkably close, and there is not a significant difference between them (i.e., [C_4C_1im][tcm] versus [C_4C_1im]-[dca]). Additionally, ideal selectivity derived from the solubility of binary systems can be inaccurate (due to round-off errors) due to the small solubility values (i.e., for HFC-125 < 0.23 and for HFC-32 < 0.35). To assess these limitations, selectivity is reevaluated using ternary diagrams coming from binary systems solubility. This is a more realistic way of analyzing selectivities for IL selection since the system includes the competition between the two HFCs (experimental solubilities of HFC-32 and HFC-125) and the IL concentration with respect to the feed (S/F ratio). The phase behavior of the ternary system, specifically, the temperature, pressure, and S/F ratio effects in selectivity of the two HFCs and the selected IL, [C_2C_1im][tcm], is analyzed. VLE boundaries were limited by fixing two specific parameters (i.e., 0.5 MPa and S/F = 6, 303.15 K and S/F = 6, or 0.5 MPa and 303.15 K) and varying the other (i.e., temperature, pressure, or S/F ratio).

4.1.4. Temperature Effect. Figure 6 illustrates the ternary phase behavior of R-410A and the IL, [C_2C_1im][tcm], at a pressure of 0.5 MPa and a constant solvent-to-feed (S/F) ratio of 6, across four different temperatures. As shown, the liquid-phase composition of the HFCs (filled circles) increases with a decreasing temperature. As the temperature increases, the vapor phase (open circles) becomes more enriched in HFC-32. Binary solubility data are placed in the plot to show the miscibility

https://doi.org/10.1021/acs.iecr.4c03268
Ind. Eng. Chem. Res. 2025, 64, 672−691

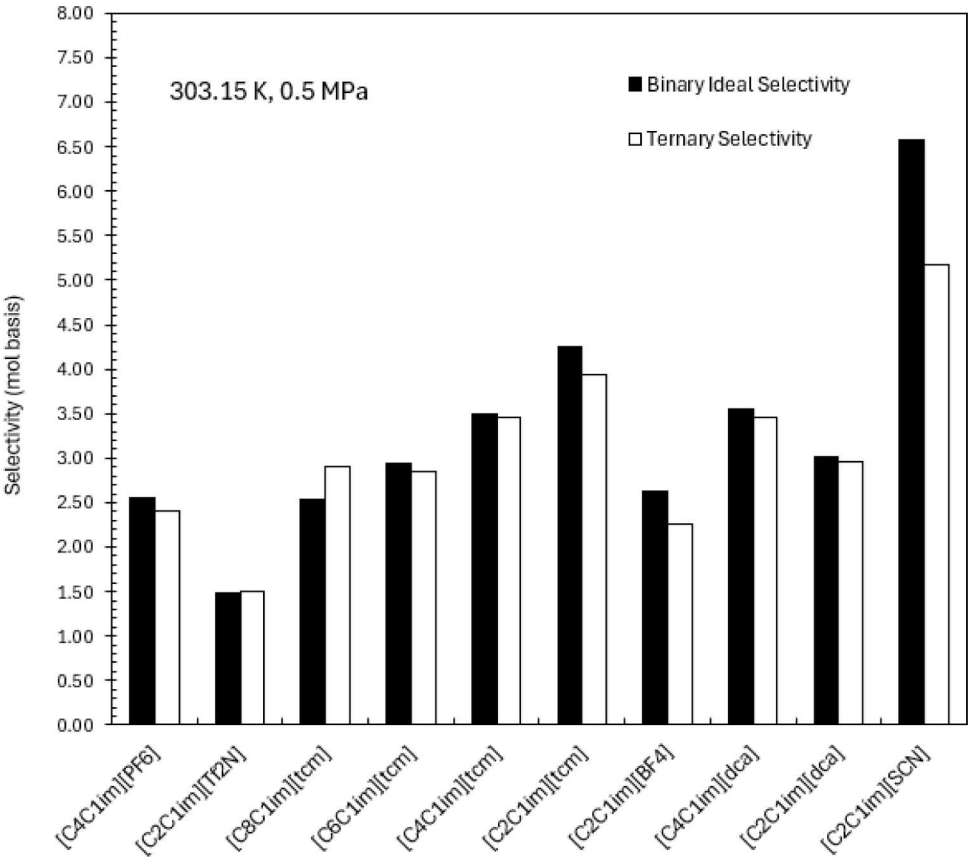

Figure 7. Selectivities, $S_{1,2}$, for binary and ternary bases at constant 303.15 K, 0.5 MPa, and S/F of 6.

boundary. The feed (at $S/F = 6$) lies between the liquid and vapor tie lines (isotherms); otherwise, a single liquid phase would exist at high S/F conditions (high IL loading). Similar qualitative behavior is found with those of the other ILs.

The actual selectivity at these different temperatures generally increases with increasing temperature, as shown in Table 5 at 283.15, 298.15, and 323.15 K. An exception was found for $[C_2C_1im][BF_4]$ whose selectivity decreased along with temperature. This finding demonstrates that not all HFCs-IL systems have the same response to temperature. Figure 7 compares the selectivity (mol basis) at 303.15 K and 0.5 MPa for ten different ILs using the idealized binary predictions versus the predicted ternary equilibrium at a S/F of 6. $[C_2C_1im][SCN]$ appears to have the highest selectivity among all the ILs at the temperature investigated; however, the difference between the binary and ternary predictions is appreciably more in comparison with the other ILs. The lowest selectivity is found for $[C_2C_1im][Tf_2N]$. Selectivities from either the binary basis (ideal) or ternary basis at 0.5 MPa and $S/F = 6$ are generally remarkably similar with an average absolute deviation of about 6%. This may indicate that an ideal binary system can be used for estimating the distillation capacity in a ternary system.

For three of the ten ILs, the predicted selectivity on a ternary (more realistic) basis was slightly lower than that predicted on a binary basis. However, one notable difference between ternary- and binary-based selectivities exhibited an error of over 10%. For example, a +15% difference was observed for $[C_8C_1im][tcm]$ at 303.15 K, indicating that the ternary system in extractive distillation may demonstrate higher selectivity than binary-based predictions would indicate. While in this specific situation the differences in selectivity between the ILs would remain qualitatively the same for IL selection studies, these discrepancies may change the analysis under other conditions, gas systems, or ILs. It should be cautioned that no ternary experimental data were available to compare these predictions of the thermodynamic model. Future work should ascertain the ability of the model for ternary predictions and subsequent process simulation.

Often, mass fraction-based units are used for solvent selection analysis. Ternary-based selectivity remains identical whether on a mole fraction or mass fraction basis. However, the idealized selectivity ($S_{1,2}^{Ideal}$) from binary and mass basis is different from that based on the mole fraction by the ratio of the molecular weights of the gases (MW_2/MW_1). Thus, there would be significant differences between the absolute values of selectivity on binary and ternary basis. Nevertheless, the qualitative trends remain the same.

Higher selectivity of HFC-125/HFC-32 in the binary than in the ternary system means that the heavy key component (HFC-32) is more soluble in the IL, or the light key component (HFC-125) is less soluble in the IL. In the ternary system, the vapor mole fractions for HFC-125 and HFC-32 are different from unity; therefore, higher selectivities suggest higher HFC-125 distribution coefficients ($K_{HFC\text{-}125}$) or lower HFC-32 distribution coefficients ($K_{HFC\text{-}125}$).

The sensitivity of temperature on selectivity can vary significantly by ionic liquids. Figure 8 illustrates the selectivity of $[C_2C_1im][tcm]$ and $[C_2C_1im][dca]$ with temperature. As shown, the selectivity with $[C_2C_1im][dca]$ is predicted to only experience a slight increase with temperature from 283.15 to 323.15 K (~3%). However, within the same temperature interval, $[C_2C_1im][tcm]$ experiences a significant selectivity

https://doi.org/10.1021/acs.iecr.4c03268
Ind. Eng. Chem. Res. 2025, 64, 672−691

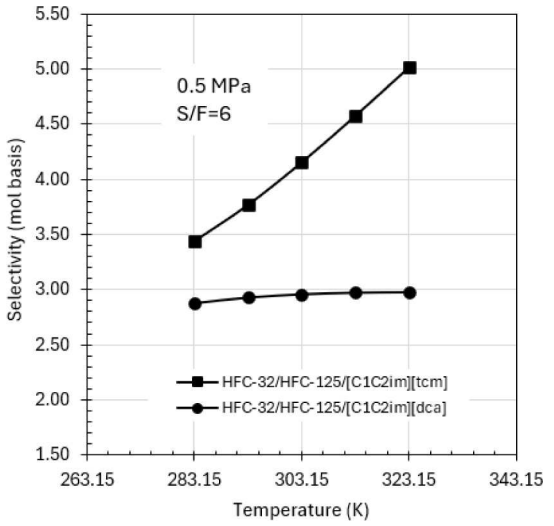

Figure 8. Temperature effect on selectivity (mol basis) for HFC-125/HFC-32/[C_2C_1im][tcm] and HFC-125/HFC-32/[C_2C_1im][dca] ternary systems at 283.15, 293.15, 303.15, 313.15, and 323.15 K at 0.5 MPa and S/F = 6 (mass basis).

increase (~62%). Understanding this temperature effect may be critical during the selection of ionic liquids. The selectivity comparison should be made within the normal temperature operations of the extractive distillation column and not necessarily some arbitrary temperature (e.g., 298.15 K, etc.).

4.1.5. Pressure Effect. In Figure 9, the ternary phase behavior of R-410A and the IL, [C_2C_1im][tcm], at a temperature of 303.15 K and a constant solvent-to-feed (S/F) ratio of 6 across four different pressures is studied. As shown, the liquid-phase composition of the HFCs (filled circles) increases with increasing pressure. As the pressure is increased, the vapor phase (open circles) becomes more enriched in HFC-125. It is interesting to find that at a pressure of 1.4 MPa, the liquid-phase composition reaches the feed composition, which indicates that the bubble point has been reached. Any pressure above 1.4 MPa will produce a single liquid phase, where all the HFC-125 and HFC-32 become miscible in the IL. Binary solubility data are included in the plot to show the miscibility boundary. The feed (at S/F = 6) lies between the liquid and vapor tie lines (constant pressure); otherwise, a single liquid phase would exist at high S/F conditions (high IL loading). Similar qualitative behavior is found with other ILs.

For the ternary systems HFC-125 (1)/HFC-32 (2)/[C_2C_1im][tcm] (3) and HFC-125 (1)/HFC-32 (2)/[C_2C_1im]-[dca] (3), selectivity decreases with pressure, as shown in Figure 10. This behavior is opposite to the temperature effect.

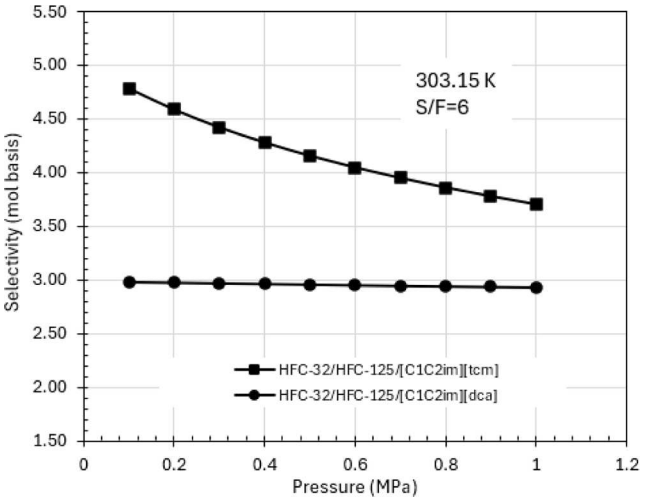

Figure 10. Pressure effect on selectivity (mol basis) for HFC-125/HFC-32/[C_2C_1im][tcm] and HFC-125/HFC-32/[C_2C_1im][dca] ternary systems at 303.15 K and S/F = 6 (mass basis).

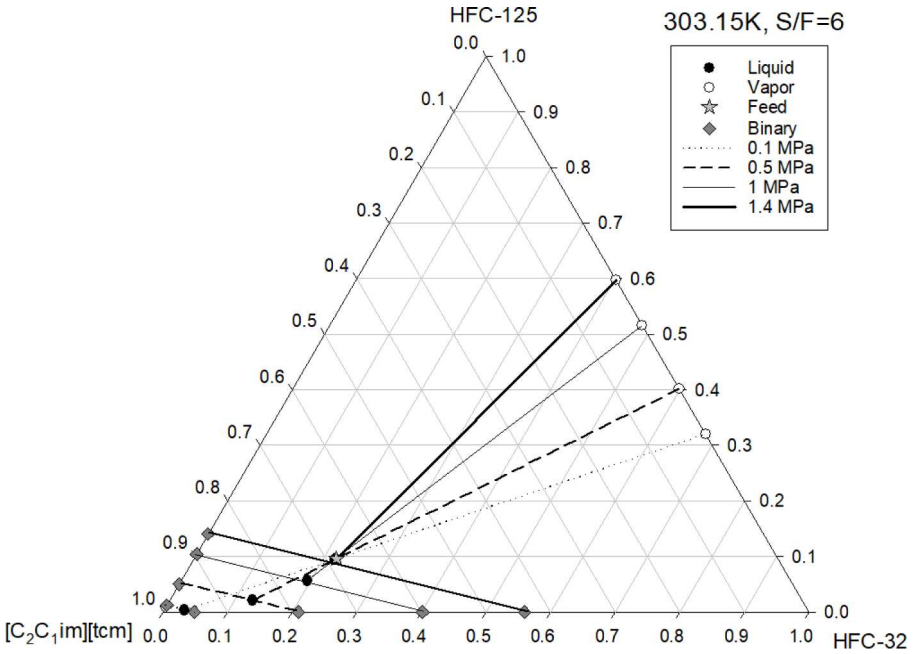

Figure 9. Pressure effect on solubility (mol basis) for HFC-125/HFC-32/[C_2C_1im][tcm] and HFC-125/HFC-32/[C_2C_1im][dca] ternary systems at 303.15 K and S/F = 6 (mass basis). Isothermal lines between the binary VLE are included to aid visualization.

https://doi.org/10.1021/acs.iecr.4c03268
Ind. Eng. Chem. Res. 2025, 64, 672−691

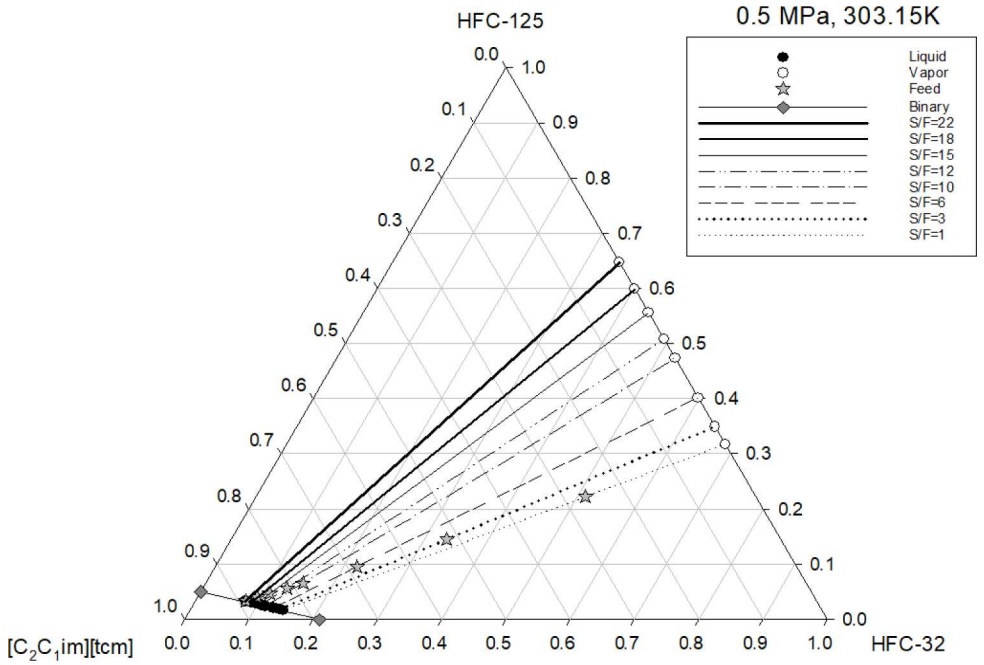

Figure 11. *S*/*F* ratio effect on solubility (mol basis) for HFC-125/HFC-32/[C_2C_1im][tcm] at *S*/*F* ratios of 1, 3, 6, 10, 12, 15, 18, and 22 (mass basis) at 0.5 MPa and 303.15 K.

Comparing the two ternary systems, pressure has a greater impact on selectivity for refrigerant blends in [C_2C_1im][tcm] than in [C_2C_1im][dca]. In the case of HFC-125/HFC-32/[C_2C_1im][dca], selectivity remains almost constant. Similar to the temperature effects, [C_2C_1im][tcm] experiences a much larger sensitivity to pressure than [C_2C_1im][dca]. This also indicates that IL selection should be based on pressures that are closer to the normal operation of an extractive distillation column, rather than a single arbitrary pressure, e.g., 0.1 MPa, etc.

4.1.6. Solvent-to-Feed Ratio Effect. The ternary phase behavior of HFC-125/HFC-32/[C_2C_1im][tcm] at 0.5 MPa and 303.15 K is shown in Figure 11 at different solvent-to-feed (*S*/*F*) ratios. The maximum possible loading (*S*/*F*) would be at the saturation conditions of the liquid phase, as indicated by the filled circles and the line connecting the two binary solubility results (diamonds). For this case, an *S*/*F* of 22 is found to be the limit where the liquid composition equals the feed composition. Thus, the loadings for VLE separations must be below this value. In general, when the S/F is changed from 1 to 12, the HFC-32 solubility decreases while the HFC-125 solubility increases.

The *S*/*F* ratio effect in selectivity is analyzed in Figure 12 for HFC-125/HFC-32/[C_2C_1im][tcm] and HFC-125/HFC-32/[C_2C_1im][dca] at 0.5 MPa and 303.15 K. Comparing the two ternary systems, the impact of *S*/*F* on refrigerant blends in [C_2C_1im][tcm] is slightly higher than in [C_2C_1im][dca]. In general, there is not a significant effect on selectivity, even across an *S*/*F* range of 1 to 12.

These trends of temperature, pressure, and *S*/*F* ratio on selectivity can help in the selection of one IL over another. In this case, comparing the results for [C_2C_1im][tcm] and [C_2C_1im][dca] has shown that an extractive distillation system that operates at higher temperatures, lower pressures, and any *S*/*F* ratio would be appropriate. However, other design parameters must be considered, such as the effect of the number of stages in the column, reflux ratio, or the feed stage. Care must be taken with the conditions (temperature and pressure) under which ILs are evaluated for separation. Some ILs have more sensitivity to

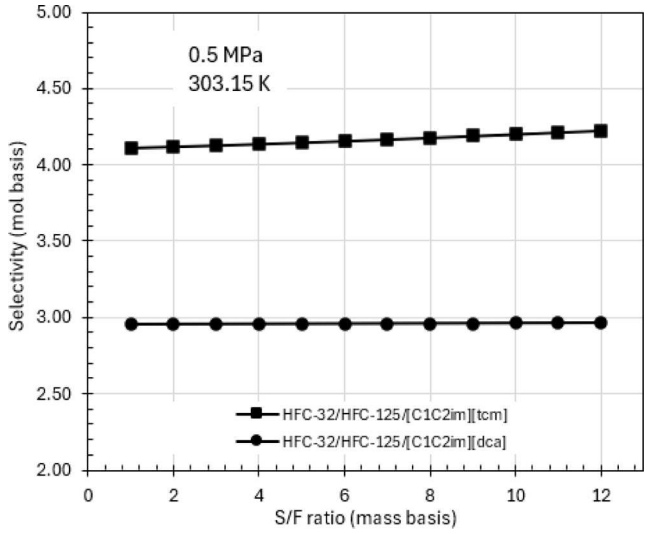

Figure 12. S/F ratio effect on selectivity for HFC-125/HFC-32/[C_2C_1im][tcm] and HFC-125/HFC-32/ [C_2C_1im][dca] at 303.15 K and 0.5 MPa.

pressure, temperature, or S/F ratio than others. In this analysis, [C_2C_1im][tcm] and [C_2C_1im][dca] have the same cations but exhibit dramatically different sensitivities to the process parameters. It can be seen that pressure and temperature affect the IL more with a higher number of cyano-groups (e.g., [C_2C_1im][tcm] (3 −CN) than [C_2C_1im][dca] (2 −CN).

4.1.7. Stability. When selecting an IL for extractive distillation, caution is needed regarding both chemical and thermal stability.[107] For example, Freire and coworkers found that [PF_6]-based ILs can undergo hydrolysis to HF under acidic conditions (e.g., pH ∼ 3) or at elevated temperatures (e.g., 343 and 373 K).[108] Likewise, Li and Pistorius concluded that the [$SCN]^-$-based ILs can produce sulfide corrosion products in the presence of certain metals such as nickel and type 304 stainless

https://doi.org/10.1021/acs.iecr.4c03268
Ind. Eng. Chem. Res. 2025, 64, 672−691

Table 6. Summary of Optimal Process Parameters for All Cases Analyzed from the Sensitivity Analysis of R-410A Separation Using $[C_2C_1im][tcm]$[a]

Case #	N_t	N_f	Column pressure (MPa)	S/F	RR	HFC-125 purity (wt %)	HFC-32 purity (wt %)	Condenser temperature (K)	Reboiler temperature (K)
1	20	12	1	7	**3**	99.75	99.75	286.43	332.32
2			1.2	6		99.75	99.75	292.91	334.83
3			**1.4**	**5**		**99.56**	**99.56**	**298.57**	**334.88**
4			1.0	6	4	99.52	99.52	286.37	325.80
5			1.0	6	5	99.78	99.78	286.44	325.89
6			1.0	5	6	99.66	99.66	286.41	318.99
7	25	15	0.9	7	3	99.77	99.77	282.82	327.14
8			1.1	6		99.85	99.85	289.81	330.52
9			1.4	5		99.89	99.89	298.66	335.01
10			0.9	7	4	99.94	99.94	282.86	327.20
11			0.9	6	5	99.89	99.89	282.85	321.00
12			0.9	5	6	99.83	99.83	282.83	314.39
13	30	18	0.9	7	3	99.92	99.92	282.86	327.20
14			1.1	6		99.96	99.96	289.83	330.56
15			1.3	5		99.88	99.88	295.89	331.34
16			0.9	6	4	99.60	99.60	282.78	320.91
17			0.9	6	5	99.97	99.97	282.87	321.03
18			0.9	5	6	99.95	99.95	282.86	314.43

[a]For all cases, the targeted purity (>99.5 wt %) of HFC-125 and HFC-32 was achieved.

steel.[102−105] We have also observed metal leaching from stainless steel with $[SCN]^-$ ILs. Ionic liquid thermal stability is considered an advantage over traditional organic solvents; however, the long-term thermal stability of ILs in an extractive distillation process must be evaluated. To prevent decomposition, the reboiler temperature should be kept below the onset temperature of degradation (temperature at which 1% degradation occurs within 10 h).[109−112] Since no thermal stability data for ILs and refrigerant mixtures were found in the literature, thermal stability data for ILs in nitrogen were used as a reference. More experimental data for thermal and chemical stability for refrigerants in ILs are needed.

4.2. Extractive Distillation Column Optimization. The extractive distillation optimization process was developed separately for each selected IL ($[C_2C_1im][dca]$ and $[C_2C_1im][tcm]$) to determine the optimal set of operating parameters. One of the main objectives is to obtain separated HFCs of at least 99.5% mass purity which is the industry standard for sale. For both ILs, 18 cases are reported that were in good agreement with the constraints and heuristics described in Section 3.1. The overall best case will be Case #3 for both ILs, which has the lowest energy usage (i.e., operational cost) and the fewest number of stages (i.e., capital cost).

Our initial hypothesis assumed that $[C_2C_1im][tcm]$ will have better performance with the lowest energy usage based on its highest selectivity and solubility with respect to $[C_2C_1im][dca]$ (see above). In our previous research group publication,[39] we achieved a R-410A separation with product purity of 99.6 wt % using $[C_4C_1im][PF_6]$. However, $[PF_6]$ ILs have stability issues that would prevent their industrial usage. Additionally, the process design was simplified, leading to an underestimated energy consumption. In this work, the extractive distillation system includes a more realistic set of operational units such as a column with reboiler and condenser, a flash unit, a heat exchanger, and a pump to provide a more accurate process evaluation.

4.2.1. R-410A Separation Using $[C_2C_1im][tcm]$. The separation of R-410A was achieved using $[C_2C_1im][tcm]$ in an extractive distillation column with a total number of stages, N_t, of 20, a feed stage, N_f, of 12, a column pressure of 1.1 MPa, a solvent-to-feed S/F ratio of 6, and a total reflux ratio, RR, of 3, obtaining 99.56 wt % of purity for HFC-32 and HFC-125, respectively. In this simulation, HFC-125, the light key component, is collected in the distillate and HFC-32, the heavy key component, is recovered from the bottoms. Additionally, 17 cases were evaluated with varying operational parameters (i.e., *Nt, P, S/F, RR*), the results are shown in Table 6. In general, an incremental increase in N_t leads to an incremental increase in the required S/F ratio, which also affects the refrigerant product purity, reaching ∼100% purity at 30 trays (N_t = 30) in the column. Likewise, incremental increases in N_t lead to a reduction in the needed pressure, P, as shown in Table 6. An increase in N_t and S/F increases the capital and operational costs, respectively, but also reduces the pressure, which lowers the operational cost. An integral economic evaluation needs to be done to implement this alternative on an industrial scale.

Incremental increases in the N_t and the S/F ratio result in higher total duties. The total duty is calculated as the sum of the absolute values of the individual duties from all energetic units (reboiler, condenser, flash, pump, and cooler). In a distillation process, the economic relationship between the energy cost and the main components revolves around optimizing energy use to achieve efficient separation. Reboiler and condenser are typically the largest energy consumers, and their energy costs are directly related to achieve the desire separation. The energy cost of the condenser can largely increase when the cooling requirements fall below 25 °C, necessitating the use of chillwater or refrigeration systems. The flash unit's energy cost is related only to the separation of HFC-32 and the IL, therefore the energy is directly affected by the heat of vaporization of HFC-32. For pumps, energy consumption is related to the pressure difference and the flow rate of the IL. Since pumps are mostly operated by electricity and the flow rates are low (60 to 100 kg/h), this operating cost is usually the lowest. In the case of coolers, the energy cost is associated with the temperature difference required to cool the IL, which leaves the flash tank and passes

https://doi.org/10.1021/acs.iecr.4c03268
Ind. Eng. Chem. Res. 2025, 64, 672−691

Table 7. Summary of the Total Duty for All Cases Analyzed from the Sensitivity Analysis of R-410A Separation Using $[C_2C_1im][tcm]$[a]

Case #	N_t	Column Pressure (MPa)	S/F	RR	Condenser Duty (kW)	Reboiler Duty (kW)	Flash Duty (kW)	Pump Duty (kW)	Cooler Duty (kW)	Total Duty (kW)
1	**20**	1.0	7	**3**	−0.71	1.98	2.45	0.11	−3.89	9.14
2		1.2	6		−0.64	1.78	2.06	0.10	−3.33	7.91
3		**1.4**	**5**		**−0.58**	**1.45**	**1.79**	**0.08**	**−2.78**	**6.68**
4		1.0	6	4	−0.86	1.59	2.45	0.09	−3.33	8.32
5		1.0	6	5	−1.01	1.74	2.45	0.09	−3.33	8.61
6		1.0	5	6	−1.13	1.40	2.37	0.07	−2.77	7.75
7	25	0.9	7	3	−0.74	1.74	2.71	0.10	−3.88	9.17
8		1.1	6		−0.67	1.61	2.25	0.09	−3.33	7.94
9		1.4	5		−0.61	1.34	1.93	0.07	−2.77	6.71
10		0.9	7	4	−0.90	1.91	2.70	0.09	−3.87	9.48
11		0.9	6	5	−1.05	1.56	2.66	0.08	−3.32	8.67
12		0.9	5	6	−1.18	1.27	2.54	0.07	−2.77	7.83
13	30	0.9	7	3	−0.74	1.74	2.70	0.09	−3.87	9.15
14		1.1	6		−0.67	1.61	2.24	0.08	−3.32	7.92
15		1.3	5		−0.60	1.34	1.92	0.07	−2.77	6.69
16		0.9	6	4	−0.90	1.41	2.66	0.08	−3.32	8.36
17		0.9	6	5	−1.05	1.56	2.66	0.08	−3.32	8.67
18		0.9	5	6	−1.18	1.27	2.54	0.07	−2.77	7.82

[a]Case #3 is found to be the optimal based on the minimal energy consumption.

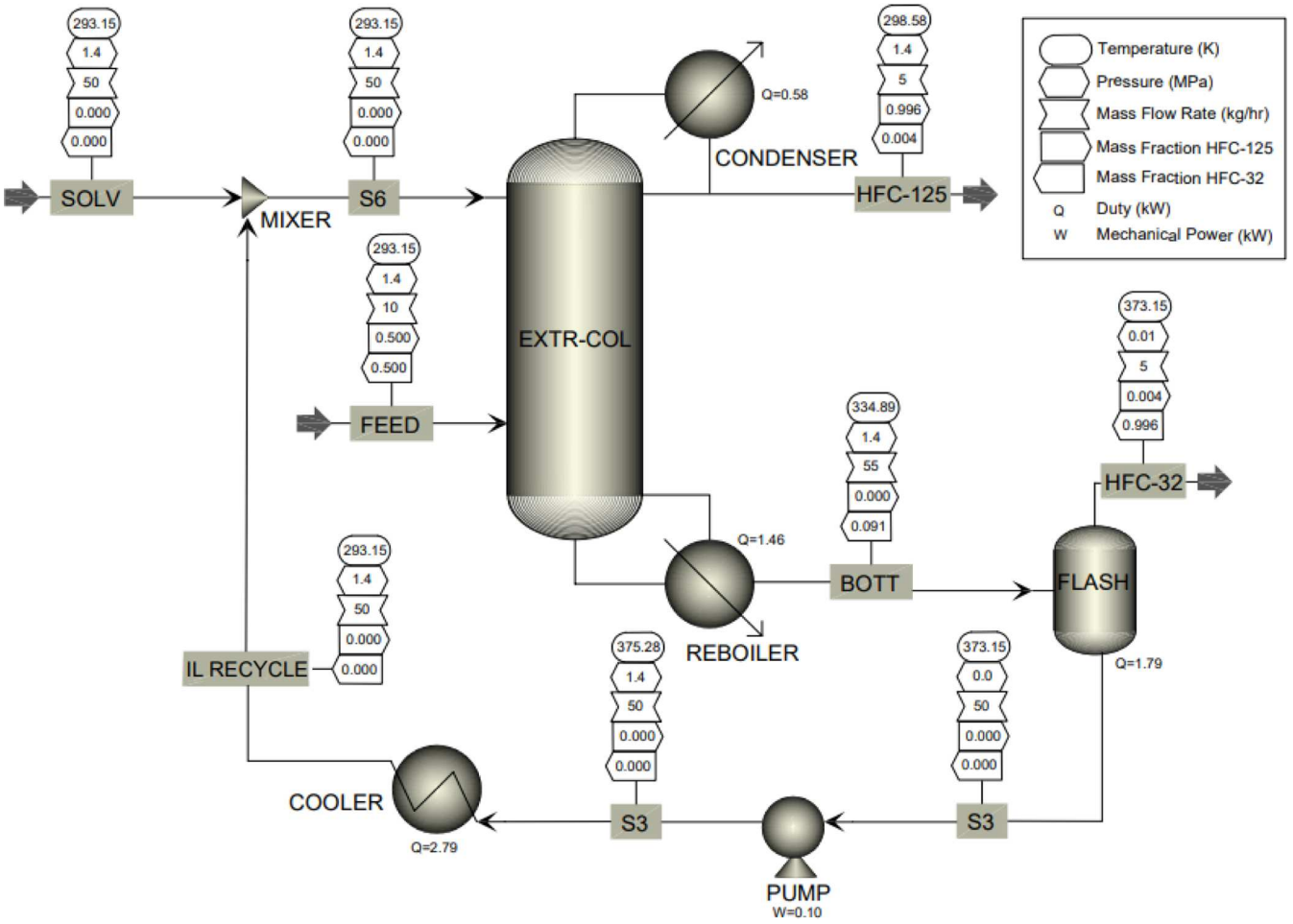

Figure 13. Process flow diagram for separating R-410A using $[C_2C_1im][tcm]$ as an entrainer in the extractive distillation system. A summary of the optimal process parameters and equipment duties is shown in Tables 6 and 7 (Case #3), respectively. The R-410A feed flow rate is set to 10 kg/h.

through the cooler before going back to the column. Minimizing energy consumption across all process units is crucial for economic efficiency, therefore optimizing the design and operation of energy-intensive equipment such as reboilers and

https://doi.org/10.1021/acs.iecr.4c03268
Ind. Eng. Chem. Res. 2025, 64, 672−691

Table 8. Summary of Optimal Process Parameters for All Cases Analyzed from the Sensitivity Analysis of R-410A Separation Using $[C_2C_1im][dca]$[a]

Case #	N_t	N_f	Column Pressure (MPa)	S/F	RR	HFC-125 Purity (wt %)	HFC-32 Purity (wt %)	Condenser Temperature (K)	Reboiler Temperature (K)
1	**20**	**12**	1	8	**3**	99.79	99.79	286.44	327.92
2			1.1	7		99.56	99.56	289.73	326.61
3			**1.4**	**6**		**99.68**	**99.68**	**298.60**	**331.50**
4			1	7	5	99.73	99.73	286.42	322.38
5			1	7	6	99.82	99.82	286.45	322.42
6			1	6	7	99.67	99.67	286.41	316.53
7	25	14	0.9	8	3	99.78	99.78	282.821	323.048
8			1.1	7		99.90	99.90	289.818	326.787
9			1.3	6		99.82	99.82	295.868	328.136
10			0.9	8	4	99.94	99.94	282.859	323.132
11			0.9	7	5	99.82	99.82	282.831	317.796
12			0.9	7	6	99.93	99.93	282.857	317.844
13	30	16	0.9	8	3	99.94	99.94	282.861	323.136
14			1.1	7		99.98	99.98	289.839	326.831
15			1.3	6		99.95	99.95	295.904	328.206
16			0.9	7	5	99.96	99.96	282.863	317.856
17			0.9	6	6	99.80	99.80	282.826	312.203
18			0.9	6	7	99.96	99.96	282.864	312.262

[a]For all cases, the targeted purity (>99.5 wt %) of HFC-125 and HFC-32 was achieved.

Table 9. Summary of the Total Duty for All Cases Analyzed from the Sensitivity Analysis of R-410A Separation Using $[C_2C_1im][dca]$[a]

Case #	N_t	Column Pressure (MPa)	S/F	RR	Condenser Duty (kW)	Reboiler Duty (kW)	Flash Duty (kW)	Pump Work (kW)	Cooler Duty (kW)	Total Duty (kW)
1	**20**	1	8	**3**	−0.71	1.92	2.90	0.11	−4.28	9.92
2		1.1	7		−0.67	1.61	2.66	0.10	−3.75	8.79
3		**1.4**	**6**		**−0.58**	**1.53**	**2.15**	**0.08**	**−3.21**	**7.55**
4		1	7	5	−1.02	1.74	2.87	0.09	−3.74	9.46
5		1	7	6	−1.17	1.89	2.87	0.09	−3.74	9.75
6		1	6	7	−1.30	1.59	2.78	0.07	−3.21	8.95
7	25	0.9	8	3	−0.74	1.68	3.17	0.10	−4.28	9.96
8		1.1	7		−0.67	1.61	2.66	0.09	−3.74	8.77
9		1.3	6		−0.61	1.40	2.29	0.07	−3.21	7.58
10		0.9	8	4	−0.90	1.85	3.16	0.09	−4.27	10.27
11		0.9	7	5	−1.06	1.55	3.09	0.08	−3.73	9.52
12		0.9	7	6	−1.22	1.71	3.09	0.08	−3.73	9.83
13	30	0.9	8	3	−0.74	1.68	3.16	0.09	−4.27	9.93
14		1.1	7		−0.67	1.61	2.65	0.08	−3.73	8.75
15		1.3	6		−0.60	1.40	2.29	0.07	−3.20	7.56
16		0.9	7	5	−1.06	1.55	3.09	0.08	−3.73	9.51
17		0.9	6	6	−1.20	1.31	2.96	0.07	−3.20	8.73
18		0.9	6	7	−1.35	1.45	2.96	0.07	−3.20	9.03

[a]Case #1 is found to be the optimal based on the minimal energy consumption.

condensers have significant importance. Results for the total energy consumption for the 18 cases evaluated are listed in Table 7. It is clear that there is a direct relationship between the N_t and the total duty. The lowest duty (6.68 kW) of the process is found for case #3 with N_t equal to 20, P of 1.4 MPa, S/F of 5, and a RR of 3. In contrast, the highest duty (9.48 kW) is found at N_t equal to 25, P of 0.9 MPa, S/F of 7, and a RR of 4.

The process flow diagram for separating R-410A using $[C_2C_1im][tcm]$ (case #3) is shown in Figure 13. In this case, the solvent is $[C_2C_1im][tcm]$ and enters the column with a flow rate of 60 kg/h at 293.15 K and 1.4 MPa. The S/F ratio for this case is 5. The feed of the column is R-410A, which enters the column with a flow rate of 10 kg/h at 293.15 K and 1.4 MPa. The mass compositions of the R-410A components in the feed stream are indicated with arrows pointing left for HFC-32 and right for HFC-125. The reboiler temperature for this case was found to be 334.89 K which is monitored with special consideration to not reach the onset temperature (443.15 K) where thermal degradation of the IL may commence. For all 18 cases evaluated, the required reboiler temperature was found to be less than 336.15 K. Figures 9S, 10S, and 10S provide the sensitivity analysis performed for determining the optimal N_f, S/F, and RR, respectively.

4.2.2. R-410A Separation Using $[C_2C_1im][dca]$. The separation of R-410A was achieved using $[C_2C_1im][dca]$ in an extractive distillation column with a total number of stages, N_t, of 20, a feed stage, N_f, of 12, a column pressure of 1.4 MPa, a solvent-to-feed ratio, S/F, of 6, and a total reflux ratio RR of 3,

https://doi.org/10.1021/acs.iecr.4c03268
Ind. Eng. Chem. Res. 2025, 64, 672−691

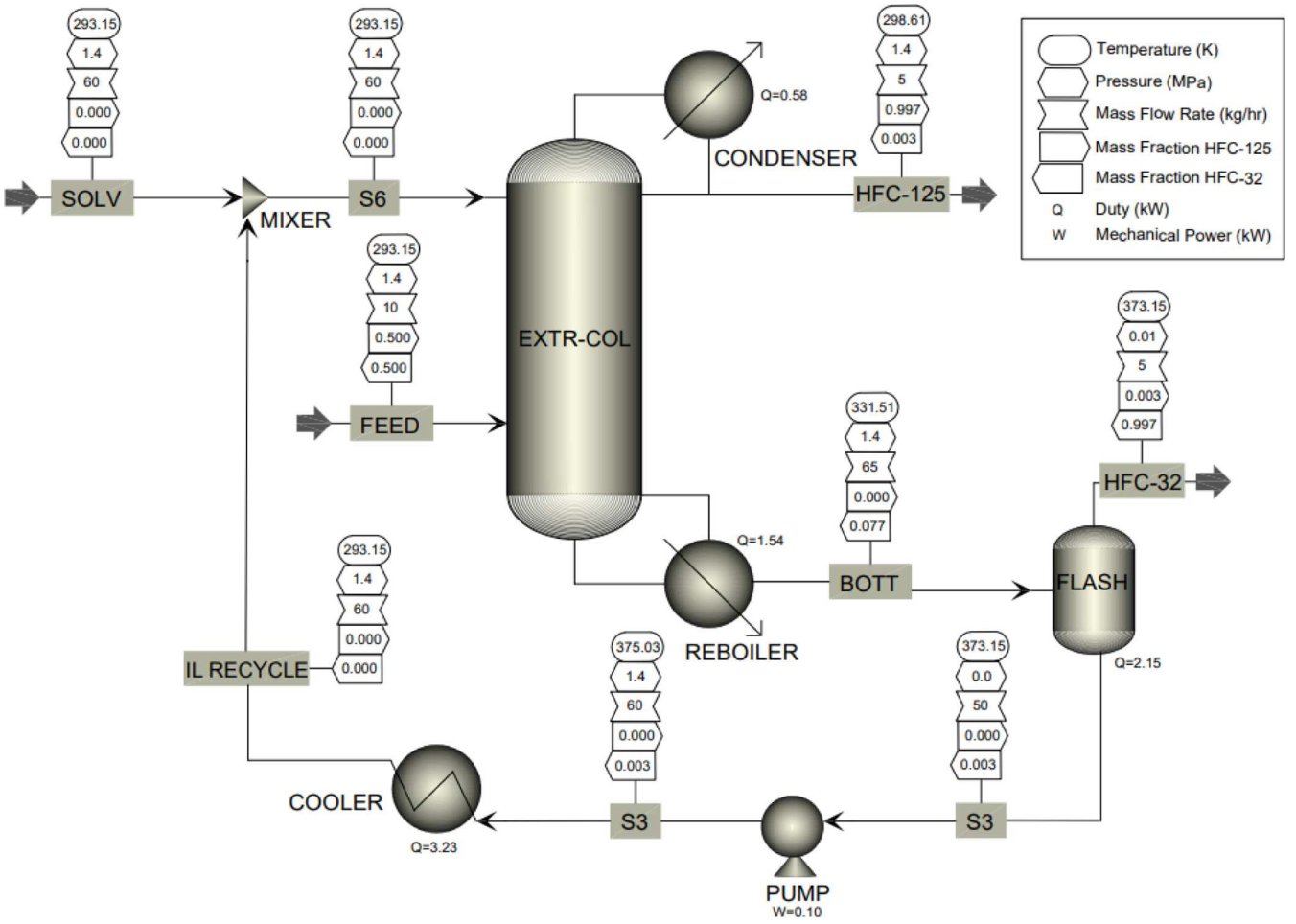

Figure 14. Process flow diagram for separating R-410A using $[C_2C_1im][dca]$ as an entrainer in an extractive distillation system. A summary of the optimal process parameters and equipment duties is shown in Tables 8 and 9 (Case #3), respectively.

Table 10. Operational Parameters for ILs Used to Separate R-410A

IL	N_t	N_f	Column P (MPa)	S/F	RR	HFC-125 purity (wt %)	HFC-32 purity (wt %)	Condenser$T$ (K)	Reboiler$T$ (K)	Reference
$[C_2C_1im][Tf_2N]$	40	17	0.90	20	4.00	95.50	95.50	281.65	388.45	39
	60	20	1.00	16	1.00	99.50	99.50	286.26	367.60	82
	28	22	1.00	14	1.50	99.56	99.56	342.30	353.70	83
$[C_2C_1im][SCN]$	18	13	1.00	6	1.40	99.50	99.50	286.00	310.00	41
	18	12	1.00	6	1.40	99.51	99.51	286.00	310.00	41
	20	10	1.00	6	2.00	99.50	99.50	286.26	309.18	82
$[C_4C_1im][PF_6]$	18	12	1.40	7	2.00	99.60	99.60	298.55	369.55	39
	27	16	0.98	12	0.24	99.50	99.5	287.50	367.50	42
	30	12	1.00	6	3.00	99.50	99.50	286.26	322.30	82
$[C_2C_1im][dca]$	20	12	1.40	6	3.00	99.68	99.68	298.60	331.50	This work
$[C_2C_1im][tcm]$	20	12	1.40	5	3.00	99.56	99.56	298.57	334.88	This work

obtaining 99.68 wt % of purity for HFC-32 and HFC-125, respectively. In this simulation, HFC-125, the light key component is collected in the distillate and HFC-32, while the heavy key component is recovered from the bottoms. Additionally, 17 cases were evaluated with varying operational parameters (i.e., N_t, P, S/F, and RR), and the results are shown in Table 8. In general, an increase in N_t leads to an increase in the refrigerant product purity, reaching 99.98 w% purity at 30 N_t in the column. Likewise, incremental increases in N_t lead to a reduction in P, as shown in Table 8. Since an increase in N_t and S/F elevates the capital and operational costs, respectively, but also reduces the pressure, which in turn reduces the operational cost, an integral economic evaluation needs to be done to implement this alternative in an industrial scale.

Again, increases in the N_t and S/F ratios produce higher total duties. Results for the total energy consumption for the 18 cases evaluated are listed in Table 9. It is clear that there is a direct relationship between N_t and the total duty. The lowest duty (7.55 kW) of the process is found for case #3 with N_t equal to 20, P of 1.4 MPa, S/F of 6, and a RR of 3. In contrast, the highest duty (10.27 kW) is found for case # 10 at N_t equal to 25, P of 0.9 MPa, S/F of 8, and a RR of 4. Therefore, case #3 was selected as

https://doi.org/10.1021/acs.iecr.4c03268
Ind. Eng. Chem. Res. 2025, 64, 672−691

Table 11. Energy Consumption for ILs Used for Separating R-410A[a]

IL	N_t	Column P (MPa)	Condenser Duty (kW)	Reboiler Duty (kW)	Flash 1 Duty (kW)	Flash 2 Duty (kW)	Cooler Duty (kW)	Pump Work (kW)	Compr./Vac. Pump Duty (kW)	Total Duty (kW) (*)	Reference
$[C_2C_1im][Tf_2N]$	40	0.90	−1.10	8.00	-	-	-	-	-	9.10	39
	60	1.00	−0.32	4.32	-	-	-	-	-	4.64	82
	28	1.00	−0.27	18.10	-	-	−18.12	0.06	-	36.56	83
$[C_2C_1im][SCN]$	18	1.00	−0.27	0.8	0.34	0.02	−0.26	0.03	-	1.71	41
	18	1.00	−0.22	0.76	0.34	0.02	−0.25	0.03	-	1.62	41
	20	1.00	−0.58	1.28	-	-	-	-	-	1.86	82
$[C_4C_1im][PF_6]$	18	1.40	−0.50	2.50	-	-	-	-	-	3.00	39
	27	0.98	−0.05	0.62	-	-	−0.68	0.05	0.4/0.03	1.83	42
	30	1.00	−0.78	1.49	-	-	-	-	-	2.27	82
$[C_2C_1im][dca]$	20	1.10	−0.58	1.53	2.15	-	−3.73	0.08	-	9.51	This work
$[C_2C_1im][tcm]$	20	1.10	−0.58	1.45	1.79	-	−2.78	0.08	-	6.68	This work

[a]Energy consumption from other references was normalized per 10 kg of R-410A processed to facilitate the comparison with this work.

the optimal case, considering the minimal N_t and the minimal total duty and, therefore, the minimal capital and operational costs.

The process flow diagram for separating R-410A using $[C_2C_1im][dca]$ case #3, is shown in Figure 14. In this case, the solvent $[C_2C_1im][dca]$ enters the column at a rate of 100 kg/h at 293.15 K and 1.4 MPa. The feed of the column is R-410A, which enters the column with a flow rate of 10 kg/h at 293.15 K and 1.4 MPa. The mass compositions of R-410A components in the feed stream are indicated with arrows pointing left for HFC-32 and right for HFC-125. The reboiler temperature for this case is found to be 331.51 K, which is monitored with special consideration to not reach the onset temperature (443.15 K) where thermal degradation of the IL starts. For all 18 cases evaluated, the reboiler temperature was found to be less than 332 K.

Figures 11S−13S provide the sensitivity analysis performed for determining the optimal N_f, S/F, and RR, respectively.

4.2.3. R-410A Separation Using Other ILs. A few studies have evaluated ILs as entrainers for separating HFC-125 and HFC-32 from R-410A. A compiled list of the operational parameters is given in Table 10. Results show the feasibility of the separation with high product purities (>99.5 wt %). It was interesting to find the remarkable difference in the S/F ratio, which can be directly correlated to selectivity. For example, the highest S/F ratios are found for $[C_2C_1im][Tf_2N]$ and $[C_4C_1im][[PF_6]$ as shown in Table 10, which have the lowest selectivities as shown in Figure 5. In general, when comparing the absorption efficiency of ILs used for separating R-410A, $[C_2C_1im][tcm]$ offers a promising alternative that reveals a lower S/F ratio (5) compared to other alternative ILs, with a relatively lower reboiler temperature (334.88 K) compared to $[C_2C_1im][Tf_2N]$ and $[C_4C_1im][PF_6]$, and a condenser temperature closer to atmospheric temperature (298.57 K) with respect to $[C_2C_1im][Tf_2N]$ and $[C_2C_1im][SCN]$. Additionally, it requires a moderate number of stages (20), a column pressure (1.4 MPa), and reflux ratio (3), in contrast to other ILs shown in Table 10.

The energy requirements for separating R-410A with different ILs are shown in Table 11. Establishing a total energy comparison can be challenging since not all the extractive distillation systems are designed with the same configuration (i.e., total versus partial condenser, one versus two flash units, etc.). However, it can be highlighted that the highest energy consumption was found for $[C_2C_1im][Tf_2N]$, which has the lowest ideal selectivity, as shown in Figure 5, which also results in the highest S/F ratio, leading to higher reboiler energy requirements. Our previous research group revealed a lower total duty for the separation of R-410A using $[C_2C_1im][[PF_6]$ (3.0 kW) than $[C_2C_1im][Tf_2N]$ (9.1 kW) per 10 kg/h of R-410 processed, as shown in Table 11. Interestingly, this study finds that using $[C_2C_1im][tcm]$ for R-410A separation produces lower reboiler temperatures. However, the total duty produced is higher because more operational units were considered (i.e., a pump, a nonadiabatic flash, and a cooler).

Asencio-Delgado et al. evaluated the R-410A separation using $[C_2C_1im][Tf_2N]$ in an equilibrium-based extractive distillation unit that includes, in addition to the column, a reboiler and a condenser; a pump, a cooler, and two adiabatic flash units. More recently, Viar et al. showed a process system for separating R-410A using $[C_2C_1im][SCN]$ with both equilibrium and rate-based models. This system included the operational units used by Asencio-Delgado but replaced the two adiabatic flash units with nonadiabatic ones. This study is more pragmatic and similar to this work. The flash units, pump, and cooler together account for a significant energy contribution to the total duty. Other researchers, such as Ye et al. included these process units in their process design, but the energy requirements were not reported. In a more rigorous process modeling, Monjur et al. presented a process design that includes the traditional extractive distillation system (EDS) described earlier, while adding a compressor and a vacuum pump for studying the R-410A separation with $[C_4C_1im][PF_6]$. The differences in normalizing the total duty for each literature system to the 10 kg/h feed rate are illustrated in Table 11.

It is important to mention that an integral economic evaluation would need to be performed to compare energy costs. For example, the electrical cost from the pump work is more expensive than the general heating costs in the reboiler, etc. In all cases, the condenser needs to cool the distillate at temperatures below 298.15 K (25 °C), which will require chilled water and/or a refrigeration system.

5. CONCLUSIONS

Solubilities from HFC-32 and HFC-125 blends (R-410A) in 10 ILs in ideal binary systems (i.e., HFC-125/IL or HFC-32/IL) were analyzed at 0.5 MPa and 303.15 K (average operational conditions in an extractive distillation system). The results

https://doi.org/10.1021/acs.iecr.4c03268
Ind. Eng. Chem. Res. 2025, 64, 672−691

indicate that cyano-based ILs have the second highest solubility difference (solubility of HFC-32 minus HFC-125) after $[C_4C_1im][PF_6]$, the most widely studied IL. It should be noted that this conclusion is based upon the ten IL systems that have available binary VLE data of both HFC-32 and HFC-125. From ideal selectivities (based on binary systems), $[C_2C_1im]$-[tcm] was selected as the best IL, exhibiting the highest selectivity-HFC-32 solubility performance in a Pareto front. $[C_2C_1im][dca]$ was another alternative to evaluate considering its relatively high selectivity, as well as to compare cyano-based ILs with the same cation. Ternary predictions were built based on ideal selectivities (binary system). Similar solubilities were found for both binary and ternary systems, which support our hypothesis that ideal binary solubilities can be generally used for predicting distillation capacity in a ternary system. The effect of temperature, pressure, and *S*/*F* ratios were studied for the two cyano-based ILs selected $[C_2C_1im][tcm]$ and $[C_2C_1im][dca]$. Results show that temperature increases selectivity, and a higher influence is shown for refrigerant blends in $[C_2C_1im][tcm]$ than in $[C_2C_1im][dca]$. On the contrary, pressure decreases selectivity; however, again a higher influence is shown for refrigerant blends in $[C_2C_1im][tcm]$ than in $[C_2C_1im][dca]$. On the other hand, an increase in the *S*/*F* ratio slightly increases selectivity, with $[C_2C_1im][tcm]$ showing a greater effect than $[C_2C_1im][dca]$.

The ILs $[C_2C_1im][tcm]$ and $[C_2C_1im][dca]$ have been found to be effective solvents for separating the azeotropic R-410 refrigerant mixture, achieving HFC-32 and HFC-125 purities greater than 99.5 wt %. By comparing the two ILs at the same operational pressure (e.g., p = 1.4 MPa), it was found that $[C_2C_1im][tcm]$ results in a lower IL *S*/*F* ratio of 5 versus 6 for $[C_2C_1im][dca]$ for a fixed *RR* of 3 and the same total number of column stages (e.g., 20) in both cases. In addition, the use of $[C_2C_1im][tcm]$ has a lower energy consumption (6.68 kW) compared to that of $[C_2C_1im][dca]$ (9.51 kW) per 10 kg/h of the R-410A feed rate. The selectivity is in good agreement with the higher reboiler temperature for $[C_2C_1im][tcm]$ (e.g., 334.88 K) compared with $[C_2C_1im][dca]$ (e.g., 331.50 K) at the same operational pressure. After comparing the performance of different ILs for separating R-410A (e.g., $[C_2C_1im][Tf_2N]$, $[C_2C_1im][SCN]$, $[C_4C_1im][PF_6]$, $[C_2C_1im][dca]$, and $[C_2C_1im][tcm]$), it was found that $[C_2C_1im][tcm]$ has lower S/F (e.g., 5) and lower number of stages (e.g., 20) versus the rest of the ILs. Cyano-based ILs, specifically $[C_2C_1im][tcm]$, are a promising option for evaluation in a pilot-scale extractive distillation column that is being operated at the University of Kansas. Further economic analysis needs to be done to estimate the capital and operating costs for a commercial scale process. In addition, more VLE data of different ILs with HFC-32 and HFC-125 are needed to continue the analysis. An important consideration is that the current simulations were performed using an equilibrium model that does not consider the effect of transport properties; therefore, these results should be considered as only an initial comparison for a process design. In the future, transport property data will be measured and a rate-based model utilizing mass and heat transfer will be performed to compare with the equilibrium-based models and pilot-scale extractive distillation results.

■ ASSOCIATED CONTENT

Supporting Information

The Supporting Information is available free of charge at https://pubs.acs.org/doi/10.1021/acs.iecr.4c03268.

Figures S1 − S14 include *PTx* diagrams and sensitivity analysis (PDF)

■ AUTHOR INFORMATION

Corresponding Author

Aaron M. Scurto − *Wonderful Institute for Sustainable Engineering, University of Kansas, Lawrence, Kansas 66045, United States; Department of Chemical and Petroleum Engineering, University of Kansas, Lawrence, Kansas 66045, United States*; Email: ascurto@ku.edu

Authors

Julia E. Espinoza Mejia − *Wonderful Institute for Sustainable Engineering, University of Kansas, Lawrence, Kansas 66045, United States; Department of Chemical and Petroleum Engineering, University of Kansas, Lawrence, Kansas 66045, United States*; orcid.org/0000-0002-6646-4276

Abdulrhman M. Arishi − *Wonderful Institute for Sustainable Engineering, University of Kansas, Lawrence, Kansas 66045, United States; Department of Chemical and Petroleum Engineering, University of Kansas, Lawrence, Kansas 66045, United States*

Mark B. Shiflett − *Wonderful Institute for Sustainable Engineering, University of Kansas, Lawrence, Kansas 66045, United States; Department of Chemical and Petroleum Engineering, University of Kansas, Lawrence, Kansas 66045, United States*; orcid.org/0000-0002-8934-6192

Complete contact information is available at: https://pubs.acs.org/10.1021/acs.iecr.4c03268

Notes

The authors declare no competing financial interest.

■ ACKNOWLEDGMENTS

Funding was provided by the National Science Foundation, Award 2213965. JEEM acknowledges the Chemical and Petroleum Department at The University of Kansas for the Summer Research Scholarship. The authors would like to acknowledge Evanna Dominic, Morela Chapman, and Joey Wiltanger, Chemical Engineering undergraduate researchers, for conducting the literature review on the physical properties of ionic liquids and helping with plots.

■ REFERENCES

(1) Chen, X.; Ding, T.; Wang, X.; Li, Z. Research on energy saving potentials using pure and zeotropic refrigerants in data center cooling systems. *Case Stud. Therm. Eng.* **2024**, *57*, 104324.

(2) McLinden, M. O.; Huber, M. L. (R)Evolution of Refrigerants. *J. Chem. Eng. Data* **2020**, *65* (9), 4176.

(3) Mussabekova, K.; Nurbayeva, A. Cooling and heating innovations: exploring the diverse applications of heat pumps. *Technobius Phy.* **2024**, *2* (2), 0014.

(4) Werner, S. District Cooling System - an overview | ScienceDirect Topics. *Encyclopedia of Energy* **2004**, 841.

(5) Vuppaladadiyam, A. K.; Antunes, E.; Vuppaladadiyam, S. S. V.; Baig, Z. T.; Subiantoro, A.; Lei, G.; Leu, S.-Y.; Sarmah, A. K.; Duan, H. Progress in the development and use of refrigerants and unintended environmental consequences. *Sci. Total Environ.* **2022**, *823*, 153670.

(6) Constable, G.; Somerville, B. *A Century of Innovation: Twenty Engineering Achievements that Transformed Our Lives*; Joseph Henry Press, 2003.

(7) Kumar, A.; Chen, M.-R.; Hung, K.-S.; Liu, C.-C.; Wang, C.-C. A Comprehensive Review Regarding Condensation of Low-GWP

Refrigerants for Some Major Alternatives of R-134a. *Processes* **2022**, *10* (9), 1882.
(8) Calm, J. M.; Hourahan, G. Refrigerant data update. *HVAC Eng.* **2007**, *79* (1), 50−64.
(9) Kim, S. W.; Park, M.; Trisna, B. A.; Lee, J. Comprehensive analysis of refrigerant R134a: Implications for estimating and managing greenhouse gas emissions. *Int. J. Refrig.* **2024**, *158*, 135.
(10) Ekins, P. *Stopping Climate Change: Policies for Real Zero*; Taylor & Francis, 2023.
(11) Saouter, E.; Gibon, T. *All You Need to Know About the Next Energy Revolution*; Springer, 2024.
(12) Langevin, J.; Wilson, E.; Snyder, C.; Narayanamurthy, R.; Miller, J.; Kaplan, K.; Reiner, M.; Risser, R.; Mahoney, M.; Geyer, J. *Decarbonizing the US Economy by 2050: a National Blueprint for the Buildings Sector*; Lawrence Berkeley National Laboratory (LBNL): Berkeley, CA, United States, 2024.
(13) Ozone-Secretariat *The Montreal Protocol on Substances that Deplete the Ozone Layer*; Ozone-Secretariat, 2000.
(14) Ozone-Secretariat. *Handbook for the International Treaties for the Protection of the Ozone Layer: vienna Convention (1985), the Montreal Protocol (1987)*; UNEP/Earthprint, 2003.
(15) Faure, M.; Lefevere, J. *Compliance with International Environmental Agreements | 9 | The Globa*; The Global Environment, 2023. .
(16) US-EPA. *Final Rule - Phasedown of Hydrofluorocarbons: restrictions on the Use of Certain Hydrofluorocarbons under Subsection (i) of the American Innovation and Manufacturing Act of 2020*; US-EPA, 2023.
(17) Booten, C.; Nicholson, S.; Mann, M. *Refrigerants: market trends and supply chain assessment*; U.S. Clean Energy Manufacturing Analysis Center,2020.
(18) Baca, K. R.; Al-Barghouti, K.; Wang, B.; Bennett, M.; Matamoros Valenciano, L.; May, T. L.; Xu, I.; Cordry, M.; Haggard, D. M.; Haas, A. G.; et al. Ionic Liquids for the Separation of Fluorocarbon Refrigerant Mixtures. *Chem. Rev.* **2024**, *124*, 5167.
(19) Rohatgi, N. D. T.; Whitmire, T. T.; Clark, R. W.*Chloride, fluoride, and acidity measurements in refrigerants;* ASHRAE 2001 Winter Meeting CD, Technical and Symposium Papers, 2001.
(20) Shiels, V.; Lyons, B. The quality of natural refrigerants: The importance of specifying high purity product sNatural Refrigerants. *Sustainable Ozone and Climate-Friendly Alternatives to HCFCs*; Proklima International, 2012, 225−236.
(21) Ali, H. M.; Kadhim, S. A.; Ibrahim, O. Evaluating Refrigerant Purity Characteristics: An Experimental Approach to Assess Impact on Vapor-Compression Refrigeration System Performance. *Int. J. Heat & Technol.* **2023**, *41* (4), 883−890.
(22) Lee, J.-H.; Choi, S.-S.; Gwak, D.-C.; Jung, Y.-A.; Lee, S.-H. Establishing methodology for evaluating refrigerant recovery and recycling equipment: institutional responses to climate change in South Korea. *J. Mater. Cycles Waste Manage.* **2018**, *20* (2), 985−994.
(23) Ozone-SecretariatRefrigeration, Air Conditioning and Heat Pumps Technical Options Committee 2018.
(24) Calm, J. M. The next generation of refrigerants − Historical review, considerations, and outlook. *Int. J. Refrig.* **2008**, *31* (7), 1123.
(25) Yancey, A. D.; Terian, S. J.; Shaw, B. J.; Bish, T. M.; Corbin, D. R.; Shiflett, M. B. A review of fluorocarbon sorption on porous materials. *Microporous Mesoporous Mater.* **2022**, *331*, 111654.
(26) Yancey, A. D.; Broom, D. P.; Roper, M. G.; Benham, M. J.; Corbin, D. R.; Shiflett, M. B. Separation of Azeotropic Hydrofluorocarbon Refrigerant Mixtures: Thermodynamic and Kinetic Modeling for Binary Adsorption of HFC-32 and HFC-125 on Zeolite 5A. *Langmuir* **2022**, *38* (35), 10836.
(27) Yancey, A. D.; Corbin, D. R.; Shiflett, M. B. Difluoromethane (HFC-32) and Pentafluoroethane (HFC-125) Sorption on Linde Type A (LTA) Zeolites for the Separation of Azeotropic Hydrofluorocarbon Refrigerant Mixtures. *Langmuir* **2022**, *38* (6), 1937.
(28) Whitehead, B. S.; Brennessel, W. W.; Brennessel, W. W.; Michtavy, S. S.; Silva, H. A.; Kim, J.; Milner, P. J.; Porosoff, M. D.; Barnett, B. R.; Whitehead, B. S.; et al. Selective adsorption of fluorinated super greenhouse gases within a metal−organic framework with dynamic corrugated ultramicropores. *Chem. Sci.* **2024**, *15* (16), 5964−5972.
(29) Zhao, Y.-L.; Li, J.-R.; Li, M.-Z.; Zhang, X.; Zhang, X.; Li, M.-Z.; Li, J.-R.; Zhao, Y.-L. Non-CO 2 greenhouse gas separation using advanced porous materials. *Chem. Soc. Rev.* **2024**, *53* (4), 2056−2098.
(30) Harders, A. N.; Dixon, S.; Hines, B.; Lundin, M.; White, W.; Shiflett, M. B. Separation of Refrigerant Gases Using a Copolymer of Perfluoro(2,2-dimethyl-1,3-dioxole) (PDD) and Vinyl Acetate (VA). *Ind. Eng. Chem. Res.* **2023**, *62* (37), 15148.
(31) Harders, A. N.; Sturd, E. R.; Vallier, J. E.; Corbin, D. R.; White, W. R.; Junk, C. P.; Shiflett, M. B. Selective separation of HFC-32 from R-410A using poly (dimethylsiloxane) and a copolymer of perfluoro (butenyl vinyl ether) and perfluoro (2, 2-dimethyl-1, 3-dioxole). *J. Membr. Sci.* **2022**, *652*, 120467.
(32) Harders, A. N.; Sturd, E. R.; Wallisch, L.; Schmidt, H.; Mendoza-Apodaca, Y.; Corbin, D. R.; White, W.; Junk, C. P.; Shiflett, M. B. S. Diffusivity, and Permeability of HFC-32 and HFC-125 in Amorphous Copolymers of Perfluoro(butenyl vinyl ether) and Perfluoro(2,2-dimethyl-1,3-dioxole). *Ind. Eng. Chem. Res.* **2023**, *62* (9), 4054−4063.
(33) Pardo, F.; Zarca, G.; Urtiaga, A. Separation of Refrigerant Gas Mixtures Containing R32, R134a, and R1234yf through Poly(ether-block-amide) Membranes. *ACS Sustainable Chem. Eng.* **2020**, *8* (6), 2548.
(34) El-Okazy, M. A.; Liu, L.; Junk, C. P.; Kathmann, E.; White, W.; Kentish, S. E. Gas separation performance of copolymers of perfluoro (butenyl vinyl ether) and perfluoro (2, 2-dimethyl-1, 3-dioxole). *J. Membr. Sci.* **2021**, *634*, 119401.
(35) Arishi, A. M.; Espinoza Mejia, J. E.; Shiflett, M. B. Separation of Azeotropic Refrigerant Mixtures: R-450A, R-456A, R-515B, and R-516A Using Phosphonium- and Imidazolium-Based Ionic Liquids. *Ind. Eng. Chem. Res.* **2024**, *63* (15), 6754.
(36) Arishi, A. M.; Shiflett, M. B. Azeotropic Refrigerant Mixture R-513A Separation Using Extractive Distillation with Ionic Liquids Entrainers. *Ind. Eng. Chem. Res.* **2023**, *62* (46), 19862.
(37) Finberg, E. A.; Cordry, M.; May, T. L.; Baca, K. R.; Shiflett, M. B. Ionic Liquid Selection for the Separation of Refrigerant Mixtures Using Extractive Distillation. *Ind. Eng. Chem. Res.* **2023**, *62* (39), 16070.
(38) Finberg, E. A.; May, T. L.; Shiflett, M. B. Multicomponent Refrigerant Separation Using Extractive Distillation with Ionic Liquids. *Ind. Eng. Chem. Res.* **2022**, *61*, 9795.
(39) Finberg, E. A.; Shiflett, M. B. Process Designs for Separating R-410A, R-404A, and R-407C Using Extractive Distillation and Ionic Liquid Entrainers. *Ind. Eng. Chem. Res.* **2021**, *60* (44), 16054−16067.
(40) Ye, G.; Wu, X.; Gao, N.; Xu, Y.; Guo, Z.; Han, X. COSMO-RS guided screening of ionic liquids for the separation of fluorinated greenhouse gases R-410A: Delving into anion, cation effects, and hydrogen bond dynamics. *Environ. Res.* **2023**, *239*, 117386.
(41) Viar, M.; Asensio-Delgado, S.; Pardo, F.; Zarca, G.; Urtiaga, A. In the quest for ionic liquid entrainers for the recovery of R-32 and R-125 by extractive distillation under rate-based considerations. *Sep. Purif. Techno.l* **2023**, *324*, 124610.
(42) Monjur, M. S.; Iftakher, A.; Hasan, M. M. F. Separation Process Synthesis for High-GWP Refrigerant Mixtures: Extractive Distillation using Ionic Liquids. *Ind. Eng. Chem. Res.* **2022**, *61* (12), 4390.
(43) Gadhiraju, V. *Cryogenic mixed refrigerant processes*; Springer, 2008. DOI: .
(44) Gerbaud, V.; Rodriguez-Donis, I.; Hegely, L.; Lang, P.; Denes, F.; You, X. Review of extractive distillation. Process design, operation, optimization and control. *Chem. Eng. Res. Des.* **2019**, *141*, 229−271.
(45) Ma, Y.; Cui, P.; Wang, Y.; Zhu, Z.; Wang, Y.; Gao, J. A review of extractive distillation from an azeotropic phenomenon for dynamic control. *Chin. J. Chem. Eng.* **2019**, *27* (7), 1510−1522.
(46) Fadia, G.; Hassiba, B.; Weifeng, S. Separation of ethanol−water mixture by extractive distillation using pyridinium-based ionic liquid 1-ethyl-3-methylpyridinium ethylsulfate. *Chem. Eng. Proc.* **2022**, *173*, 108815.
(47) Wang, C.; Zhuang, Y.; Dong, Y.; Liu, L.; Zhang, L.; Du, J. Conceptual design of sustainable extractive distillation processes combining preconcentration and extractive distillation functions for

https://doi.org/10.1021/acs.iecr.4c03268
Ind. Eng. Chem. Res. 2025, 64, 672−691

separating ternary multi-azeotropic mixture. *Chem. Eng. Sci.* **2022**, *263*, 118088.
(48) Varyemez, H. S.; Kaymak, D. B. Effect of operating pressure on design of extractive distillation process separating DMC-MeOH azeotropic mixture. *Chem. Eng. Res. Des.* **2022**, *177*, 108−116.
(49) Melfi, D. T.; Scurto, A. M. Viscosity of imidazolium ionic liquids and mixtures of ILs from entropy scaling using the PC-SAFT and ePC-SAFT equations of state. *J. Mol. Liq.* **2024**, *401*, 124500.
(50) Al-Barghouti, K. S.; Scurto, A. M. Thermal Conductivity of 1-Alkyl-3-methylimidazolium [Tf2N] Ionic Liquids and Compressed 1,1,1,2-Tetrafluoroethane (R-134a). *J. Chem. Eng. Data* **2022**, *67* (8), 1796.
(51) Baca, K. R.; Harders, A. N.; Starvaggi, N.; Wang, Y.; Valenciano, L. M.; Bennett, M.; Haggard, D. M.; Xu, I.; Pentzer, E.; Shiflett, M. B. *Phase Equilibria and Diffusivities of HFC-32 and HFC-125 in Encapsulated Ionic Liquids AIChE*; 2023 AichE Annual Meeting, 2023.
(52) Mellein, B. R.; Scurto, A. M.; Shiflett, M. B. Gas solubility in ionic liquids. *Curr. Opin. Green Sustain.* **2021**, *28*, 100425.
(53) Shiflett, M. B.; Scurto, A. M. Ionic liquids: current state and future directions. *Ionic Liquids: current State And Future Directions* **2017**, *1250*, 1−13.
(54) Shiflett, M. B.; Harmer, M. A.; Junk, C. P.; Yokozeki, A. Solubility and Diffusivity of Difluoromethane in Room-Temperature Ionic Liquids. *J. Chem. Eng. Data* **2006**, *51* (2), 483.
(55) Shiflett, M. B.; Yokozeki, A.; Knapp, J. P. *Process for the separation of fluorocarbons using ionic liquids* US 7,964,760 B2, 2011.
(56) Faundez, C. A.; Barrientos, L. A.; Valderrama, J. O. Modeling and thermodynamic consistency of solubility data of refrigerants in ionic liquids. *Int. J. Refrig.* **2013**, *36* (8), 2242−2250.
(57) Sosa, J. E.; Ribeiro, R. P. P. L.; Castro, P. J.; Mota, J. P. B.; Araujo, J. M. M.; Pereiro, A. B. Absorption of Fluorinated Greenhouse Gases Using Fluorinated Ionic Liquids. *Ind. Eng. Chem. Res.* **2019**, *58* (45), 20769−20778.
(58) Sun, Y. J.; Di, G. L.; Wang, J.; Hu, Y. S.; Wang, X. P.; He, M. G. Gaseous solubility and thermodynamic performance of absorption system using R1234yf/IL working pairs. *Appl. Therm. Eng.* **2020**, *172*, 115161.
(59) Asensio-Delgado, S.; Viar, M.; Pardo, F.; Zarca, G.; Urtiaga, A. Gas solubility and diffusivity of hydrofluorocarbons and hydrofluoroolefins in cyanide-based ionic liquids for the separation of refrigerant mixtures. *Fluid Phase Equilib.* **2021**, *549*, 113210.
(60) Kim, Y. J.; Kim, S.; Joshi, Y. K.; Fedorov, A. G.; Kohl, P. A. Thermodynamic analysis of an absorption refrigeration system with ionic-liquid/refrigerant mixture as a working fluid. *Energy* **2012**, *44* (1), 1005−1016.
(61) Hekayati, J.; Roosta, A.; Javanmardi, J. Thermodynamic modeling of refrigerants solubility in ionic liquids using original and ϵ*-Modified Sanchez−Lacombe equations of state. *Fluid Phase Equilib.* **2015**, *403*, 14−22.
(62) Ren, W.; Scurto, A. M. Phase equilibria of imidazolium ionic liquids and the refrigerant gas, 1,1,1,2-tetrafluoroethane (R-134a). *Fluid Phase Equilib.* **2009**, *286* (1), 1−7.
(63) Ren, W.; Scurto, A. M. Global phase behavior of imidazolium ionic liquids and compressed 1, 1, 1, 2-tetrafluoroethane (R-134a). *AichE J.* **2009**, *55* (2), 486−493.
(64) Morais, A. R. C.; Harders, A.; Baca, K. R.; Olsen, G. M.; Befort, B. J.; Dowling, A. W.; Maginn, E. J.; Shiflett, M. B. Phase Equilibria, Diffusivities, and Equation of State Modeling of HFC-32 and HFC-125 in Imidazolium-Based Ionic Liquids for the Separation of R-410A. *Ind. Eng. Chem. Res.* **2020**, *59* (40), 18222.
(65) Sun, Y.; Zhang, Y.; Di, G.; Wang, X.; Prausnitz, J. M.; Jin, L. Vapor−liquid equilibria for R1234ze (E) and three imidazolium-based ionic liquids as working pairs in absorption−refrigeration cycle. *J. Chem. Eng. Data* **2018**, *63* (8), 3053−3060.
(66) Shiflett, M. B.; Yokozeki, A. Solubility and diffusivity of hydrofluorocarbons in room-temperature ionic liquids. *AichE J.* **2006**, *52* (3), 1205−1219.
(67) Shiflett, M. B.; Yokozeki, A. Vapor-liquid-liquid equilibria of hydrofluorocarbons+1-butyl-3-methylimidazolium hexafluorophosphate. *J. Chem. Eng. Data* **2006**, *51* (5), 1931−1939.
(68) Yokozeki, A.; Shiflett, M. B. Global phase behaviors of trifluoromethane in ionic liquid [bmim][PF6]. *AichE J.* **2006**, *52* (11), 3952.
(69) Shiflett, M. B.; Yokozeki, A. Separation of difluoromethane and pentafluoroethane by extractive distillation using ionic liquid. *Chimica Oggi-Chem.* **2006**, *24* (2), 28−30.
(70) Shiflett, M. B.; Yokozeki, A. Solubility differences of halocarbon isomers in ionic liquid [emim][Tf2N]. *J. Chem. Eng. Data* **2007**, *52* (5), 2007−2015.
(71) Shiflett, M. B.; Maginn, E. J. The solubility of gases in ionic liquids. *AichE J.* **2017**, *63* (11), 4722−4737.
(72) Qin, H.; Cheng, J.; Yu, H.; Zhou, T.; Song, Z. Hierarchical ionic liquid screening integrating COSMO-RS and aspen plus for selective recovery of hydrofluorocarbons and hydrofluoroolefins from a refrigerant blend. *Ind. Eng. Chem. Res.* **2022**, *61* (11), 4083−4094.
(73) Sosa, J. E.; Santiago, R.; Redondo, A. E.; Avila, J.; Lepre, L. F.; Gomes, M. C.; Araújo, J. O. M.; Palomar, J.; Pereiro, A. B. Design of ionic liquids for fluorinated gas absorption: COSMO-RS selection and solubility experiments. *Environ. Sci. Technol.* **2022**, *56* (9), 5898−5909.
(74) Wang, N.; Zhang, Y.; Al-Barghouti, K. S.; Kore, R.; Scurto, A. M.; Maginn, E. J. Structure and dynamics of hydrofluorocarbon/ionic liquid mixtures: an experimental and molecular dynamics study. *J. Phys. Chem. B* **2022**, *126* (41), 8309−8321.
(75) Agbodekhe, B.; Marin-Rimoldi, E.; Zhang, Y.; Dowling, A. W.; Maginn, E. J. Assessment and Ranking of Difluoromethane (R32) and Pentafluoroethane (R125) Interatomic Potentials Using Several Thermophysical and Transport Properties Across Multiple State Points. *J. Chem. Eng. Data* **2024**, *69* (2), 427−444.
(76) Asensio-Delgado, S.; Pardo, F.; Zarca, G.; Urtiaga, A. Machine learning for predicting the solubility of high-GWP fluorinated refrigerants in ionic liquids. *J. Mol. Liq.* **2022**, *367*, 120472.
(77) Chu, J.; Zhang, Z.; Liu, X.; He, M. Estimating the solubility of HFC/HFO in ionic liquids from molecular structure using machine learning method. *Chem. Eng. Res. Des.* **2022**, *184*, 315−325.
(78) Sujatha, I.; Venkatarathnam, G. Comparison of performance of a vapor absorption refrigeration system operating with some hydrofluorocarbons and hydrofluoroolefins as refrigerants along with ionic liquid [hmim][TF2N] as the absorbent. *Int. J. Refrig.* **2018**, *88*, 370−382.
(79) Vieira, N. S.; Bastos, J. C.; Hermida-Merino, C.; Pastoriza-Gallego, M. J.; Rebelo, L. P.; Piñeiro, M. M.; Araújo, J. M.; Pereiro, A. B. Aggregation and phase equilibria of fluorinated ionic liquids. *J. Mol. Liq.* **2019**, *285*, 386−396.
(80) Viar, M.; Asensio-Delgado, S.; Pardo, F.; Zarca, G.; Urtiaga, A. Solubility of difluoromethane (R-32) and pentafluoroethane (R-125) in 1-alkyl-3-methylimidazolium tricyanomethanide ionic liquids. *Fluid Phase Equilib.* **2024**, *577*, 113983.
(81) Velders, G. J. M.; Fahey, D. W.; Daniel, J. S.; McFarland, M.; Andersen, S. O. The large contribution of projected HFC emissions to future climate forcing. *Proc. Natl. Acad. Sci. U.S.A.* **2009**, *106* (27), 10949.
(82) Ye, G.; Ye, M.; Wu, X.; Yan, Y.; Ouyang, H.; Han, X. Extractive distillation process using organic and ionic liquids for the separation of high-GWP refrigerant R410A: A thermodynamic and techno-economic assessment. *Chem. Eng. Res. Des.* **2023**, *197*, 558−571.
(83) Asensio-Delgado, S.; Jovell, D.; Zarca, G.; Urtiaga, A.; Llovell, F. Thermodynamic and process modeling of the recovery of R410A compounds with ionic liquids. *Int. J. Refrig.* **2020**, *118*, 365−375.
(84) ACHR-Institute *AHRI STANDARD 700−2019 Standard for Specifications for Refrigerants; 2111 Wilson Boulevard, suite 500*; ACHR-Institute: Arlington, VA 22201, USA, 2019.
(85) Valderrama, J. O.; Robles, P. A. Critical Properties, Normal Boiling Temperatures, and Acentric Factors of Fifty Ionic Liquids. *Ind. Eng. Chem. Res.* **2007**, *46* (4), 1338−1344.
(86) Valderrama, J. O.; Rojas, R. E. Critical Properties of Ionic Liquids. *Revisited. Ind. Eng. Chem. Res.* **2009**, *48* (14), 6890−6900.

https://doi.org/10.1021/acs.iecr.4c03268
Ind. Eng. Chem. Res. 2025, 64, 672−691

(87) Shariati, A.; Ashrafmansouri, S.-S.; Osbuei, M. H.; Hooshdaran, B. Critical properties and acentric factors of ionic liquids. *Korean J. Chem. Eng.* **2013**, *30* (1), 187−193.
(88) Mondal, T.; Samanta, P. Study of Physicochemical Properties of Ionic Liquids. In *Ionic Liquids in Synthesis*; Wiley, 2023.
(89) Mathias, P. M.; Klotz, H. C.; Prausnitz, J. M. Equation-of-State Mixing Rules for Multicomponent Mixtures - the Problem of Invariance. *Fluid Phase Equilib.* **1991**, *67*, 31−44.
(90) Mathias, P. M.; Boston, J. F.; Watanasiri, S. Effective utilization of equations of state for thermodynamic properties in process simulation. *AichE J.* **1984**, *30* (2), 182.
(91) Al-Barghouti, K. S.; Baca, K. R.; Shiflett, M. B.; Scurto, A. M. Phase Equilibrium and Transport Properties of the Ionic Liquid 1-Ethyl-3-methylimidazolium Bis(trifluoromethylsulfonyl)amide and Compressed Difluoromethane and Pentafluoroethane. *Ind. Eng. Chem. Res.* **2024**, *63*, 1151−1169.
(92) Rubio, R. G. R.; Renuncio, J. A. R.; Peña, M. D. Regression of vapor-liquid equilibrium data based on application of the maximum-likelihood principle. *Fluid Phase Equilib.* **1983**, *12* (3), 217−234.
(93) Al-Malah, K. I. *Aspen plus: Chemical engineering applications*; John Wiley & Sons, 2022.
(94) Schefflan, R. *Teach yourself the basics of Aspen Plus*; John Wiley & Sons, 2016.
(95) Haydary, J. *Chemical process design and simulation: Aspen Plus and Aspen Hysys applications*; John Wiley & Sons, 2019.
(96) Asensio-Delgado, S.; Pardo, F.; Zarca, G.; Urtiaga, A. Enhanced absorption separation of hydrofluorocarbon/hydrofluoroolefin refrigerant blends using ionic liquids. *Sep. Purif. Tech.* **2020**, *249*, 117136.
(97) Al-Malah, K. I. M. Flash Separation and Distillation Columns. In *Aspen Plus®*; Wiley, 2016. DOI: .
(98) Rafil, E. Physical property estimation and phase behavior for process simulation. In *Chemical Engineering Process Simulations*; Elsevier, 2023. DOI: .
(99) Wooster, T. J.; Johanson, K. M.; Fraser, K. J.; Macfarlane, D. R.; Scott, J. L. Thermal degradation of cyano containing ionic liquids. *Green Chem.* **2006**, *8* (8), 691.
(100) Cao, Y.; Mu, T. Comprehensive Investigation on the Thermal Stability of 66 Ionic Liquids by Thermogravimetric Analysis. *Ind. Eng. Chem. Res.* **2014**, *53* (20), 8651−8664.
(101) Anthony, J. L.; Maginn, E. J.; Brennecke, J. F. Solubilities and Thermodynamic Properties of Gases in the Ionic Liquid 1-n-Butyl-3-methylimidazolium Hexafluorophosphate. *J. Phys. Chem. B* **2022**, *106* (29), 7315−7320.
(102) Pistorius, P. C.; Li, W. *Accelerated corrosion of stainless steel in thiocyanate-containing solutions*; Carnegie Mellon Univ., 2012. DOI: .
(103) Li, W.; Pistorius, P. C. Effects of Thiocyanate on Anodic Dissolution of Iron, Chromium, Nickel and Type 304 Stainless Steel: I. Electrochemical Measurements and Surface Morphology. *J. Electrochem. Soc.* **2012**, *159* (11), C513−C518.
(104) Li, W.; Pistorius, P. C. Effects of Thiocyanate on Anodic Dissolution of Iron, Chromium and Type 430 Stainless Steel. *J. Electrochem. Soc.* **2012**, *159* (3), C114−C122.
(105) Li, W.; Pistorius, P. C. Effects of Thiocyanate on Anodic Dissolution of Iron, Chromium, Nickel and Type 304 Stainless Steel: II. Surface Analysis by XPS. *J. Electrochem. Soc.* **2012**, *159* (11), C519−C524.
(106) Baca, K. R.; Broom, D. P.; Roper, M. G.; Benham, M. J.; Shiflett, M. B. First Measurements for the Simultaneous Sorption of Difluoromethane and Pentafluoroethane Mixtures in Ionic liquids Using the Integral Mass Balance Method. *Ind. Eng. Chem. Res.* **2022**, *61* (61), 9774.
(107) Wang, B.; Qin, L.; Mu, T.; Xue, Z.; Gao, G. Are Ionic Liquids Chemically Stable? *Chem. Rev.* **2017**, *117* (10), 7113.
(108) Freire, M. G.; Neves, C. M. S. S.; Marrucho, I. M.; Coutinho, J. A. P.; Fernandes, A. M. Hydrolysis of Tetrafluoroborate and Hexafluorophosphate Counter Ions in Imidazolium-Based Ionic Liquids†. *J. Phys. Chem. A* **2010**, *114* (11), 3744.
(109) Chen, Y.; Mu, T. Thermal Stability of Ionic Liquids. In *Encyclopedia of Ionic Liquids*; Springer, 2019.
(110) Parajó, J.; Villanueva, M.; Salgado, J.Thermal stability of ionic liquids*Ionic Liquids: Synthesis, Properties, Technologies and Applications*-Walter de Gruyter GmbH201941−16
(111) Cao, Y. Y.; Mu, T. C. Comprehensive Investigation on the Thermal Stability of 66 Ionic Liquids by Thermogravimetric Analysis. *Ind. Eng. Chem. Res.* **2014**, *53* (20), 8651−8664.
(112) Kosmulski, M.; Gustafsson, J.; Rosenholm, J. B. Thermal stability of low temperature ionic liquids revisited. *Thermochim. Acta* **2004**, *412* (1−2), 47−53.

https://doi.org/10.1021/acs.iecr.4c03268
Ind. Eng. Chem. Res. 2025, 64, 672−691